

# Interpreting the mean surface density of companions in star-forming regions

Matthew R. Bate<sup>1</sup>, Cathie J. Clarke<sup>2</sup>, and Mark J. McCaughrean<sup>3</sup>

<sup>1</sup> Max-Planck-Institut für Astronomie, Königstuhl 17, D-69117 Heidelberg, Germany

<sup>2</sup> Institute of Astronomy, Madingley Road, Cambridge CB3 0HA

<sup>3</sup> Max-Planck-Institut für Radioastronomie, Auf dem Hügel 69, D-53121 Bonn, Germany

arXiv:astro-ph/9804154v1 16 Apr 1998

9 April 2021

## ABSTRACT

We study the interpretation of the mean surface density of stellar companions as a function of separation (or, equivalently, the two point correlation function of stars) in star-forming regions. First, we consider the form of the functions for various simple stellar distributions (binaries, global density profiles, clusters, and fractals) and the effects of survey boundaries.

Following this, we study the dependencies of the separation at which a transition from the binary to the large-scale clustering regime occurs. Larson (1995) found that the mean surface density of companions follows different power-law functions of separation in the two regimes. He identified the transition separation with the typical Jeans length in the molecular cloud. However, we show that this is valid only for special cases. In general, the transition separation depends on the volume density of stars, the depth of the star-forming region, the volume-filling nature of the stellar distribution, and on the parameters of the binaries. Furthermore, the transition separation evolves with time. We also note that in young star-forming regions, binaries with separations greater than the transition separation may exist, while in older unbound clusters which have expanded significantly, the transition contains a record of the stellar density when the stars formed.

We then apply these results to the Taurus-Auriga, Ophiuchus, and Orion Trapezium star-forming regions. We find that while the transition separation in the Taurus-Auriga star-forming region may indicate a typical Jeans length, this is not true of the Orion Trapezium Cluster. We caution against over-interpreting the mean surface density of stellar companions; while Larson showed that Taurus-Auriga is consistent with the stars having a fractal large-scale distribution we show that Taurus-Auriga is also consistent with stars being grouped in non-hierarchical clusters. We also argue that to make a meaningful study of the stellar distribution in a star-forming region requires a relatively complete stellar survey over a large area. Such a survey does not currently exist for Ophiuchus. Finally, we show that there is no evidence for sub-clustering or fractal structure in the stars of the Orion Trapezium Cluster. This is consistent with the fact that, if such structure were present when the stars formed, it would have been erased by the current age of the cluster due to the stellar velocity dispersion.

**Key words:** stars: formation – stars: pre-main-sequence – stars: statistics – open clusters and associations: general – binaries: general

## 1 INTRODUCTION

Stars generally do not form in isolation. Instead, on small scales, they frequently form as members of bound binary or higher-order multiple systems (e.g. Duquennoy & Mayor 1991; Mayor et al. 1992; Fischer & Marcy 1992; Ghez, Neugebauer, & Matthews 1993; Leinert et al. 1993; Simon

et al. 1995), while on larger scales they are often members of associations or clusters of stars (e.g. Gomez et al. 1993; Lada, Strom, & Myers 1993; Zinnecker, McCaughrean, & Wilking 1993). Studying the clustering properties of stars on different length scales may help to determine what processes are involved in their formation.

Gomez et al. (1993) found that the pre-main-sequence

stars in the Taurus-Auriga molecular cloud are not randomly distributed, but instead are in small associations of  $\sim 15$  stellar systems within radii of  $\sim 0.5 - 1.1$  pc. As one method of analysing the spatial distribution of stars, Gomez et al. determined the two-point angular correlation function and found that it could be represented by a single power-law over separations from 0.005 to 5 pc, implying that stars are clustered self-similarly. However, they also found weak evidence that two-point angular correlation function may be better represented by two different power laws with a break at  $\approx 0.05$  pc.

Using data from searches for binary companions to pre-main-sequence stars in the Taurus-Auriga molecular cloud, Larson (1995) extended the two-point angular correlation function to smaller separations than Gomez et al. (1993) and demonstrated that, indeed, there is a break at  $\approx 0.04$  pc. Rather than using the standard two-point angular correlation function, Larson used the closely-related mean surface density of companions (MSDC) (see Section 2). The MSDC has the advantage that no normalisation is required, whereas the two point correlation function must be normalised by the average density in the survey area which can be difficult to determine if the stars are clustered.

Larson (1995) found that, for stars in the Taurus-Auriga molecular cloud, the MSDC has a power-law slope of  $\approx -0.6$  on large scales, but steepens below  $\approx 0.04$  pc with a slope of  $\approx -2$  on small scales. The fact that a break occurs indicates that a single scale-free process is not responsible for the formation of stars on both scales. The power-law slope of  $\approx -0.6$  on large scales is due to the clustering of stellar systems that Gomez et al. (1993) studied. Furthermore, Larson pointed out that a power-law slope of  $-0.6$  means that the number of stars within an angular distance  $\theta$  of an average star increases as  $\theta^{1.4}$  and, thus, the distribution of stars on this scale can be described as a fractal point distribution with dimension 1.4. Larson identified the power-law slope of  $-2$  for small angular separations with the distribution of binary separations, since stellar pairs closer than 0.04 pc in Taurus-Auriga are typically mutually bound. However, the power-law slope of  $\approx -2$  is not due to a fractal distribution. Rather, it results from the fact that the frequency distribution of binary separations is roughly uniform in log-separation (Duquennoy & Mayor 1991). Finally, Larson noted that the length scale of  $\approx 0.04$  pc is essentially equal to the typical Jeans length in the Taurus-Auriga molecular cloud. Thus, Larson associated the location of the break in the MSDC with the Jeans length, speculating that companions with separations smaller than this formed due to the fragmentation of a single collapsing molecular cloud core, while on larger scales stars are grouped self-similarly due to hierarchical structure in the progenitor molecular clouds.

Following Larson's analysis of the Taurus-Auriga star-forming region (SFR), Simon (1997) considered the spatial distribution of stars in the Ophiuchus and Orion Trapezium regions. As with Taurus-Auriga, a break was found in the MSDC for each region. On small scales, both Ophiuchus and the Orion Trapezium could be fit by power laws with slopes of  $\approx -2$ . On large scales, flatter power laws were required of  $-0.5 \pm 0.2$  for Ophiuchus and  $-0.2 \pm 0.2$  for the Orion Trapezium. However, the break between the two regimes was found to occur at  $\approx 400$  AU for the Orion Trapezium and  $\approx 5000$

AU for Ophiuchus, compared to  $\approx 10000$  AU (taking the mean of Simon's and Larson's results) for Taurus-Auriga. Simon concluded that all three SFRs had similar distributions of binary separations and similar fractal structure on large scales, but that the location of the break seemed to depend not only on the Jeans length, but also on the stellar density of the SFR.

Finally, Nakajima et al. (1998) considered the MSDC of stars in the Orion, Ophiuchus, Chamaeleon, Vela, and Lupus star-forming regions. Again, for those regions where the survey data extends to small enough separations, they find a break in the MSDC with a power-law slope of  $\approx -2$  on small scales and power-law slopes ranging from  $-0.15$  to  $-0.82$  on large scales. The location of the break was also found to vary from a minimum of  $\approx 1000$  AU to a maximum of  $\approx 30000$  AU. Nakajima et al. also considered the nearest-neighbour distributions for each of the regions and found that when the nearest-neighbour distribution could be fit well by a Poisson distribution, the MSDC had a power-law index close to zero on large-scales, while when the nearest-neighbour distribution was broader than the Poisson distribution, the MSDC had a large, negative power-law index. They interpreted this as evidence that the MSDC may indicate a star formation history in the region rather than the presence of self-similar spatial structure; if the stars have a range of ages, the older stars typically will be more dispersed than the younger stars resulting a spread in the distribution of separations of nearest neighbours and a range of stellar surface density which provides the slope of the large-scale MSDC.

Motivated by these papers, we make a careful study of the interpretation of the mean surface density of companions (MSDC) of star-forming regions. Amongst other goals, we wish to determine the relationship of the break between the binary and large-scale regimes to the Jeans length and the stellar density in star-forming regions. We also want to determine how sensitive the MSDC is to detecting sub-structure in a stellar distribution and, when detected, what can be said about the form of the sub-structure (e.g. whether the sub-structure is self-similar or not) and how robust the result is.

In Section 2 we consider the calculation of the MSDC function, handling of survey boundaries, and the results for simple stellar distributions (binaries, global density profiles, clusters, and fractals). In Section 3 we derive the dependencies of the break between the binary and large-scale regimes, and show that the separation at which the break occurs can only be identified with the Jeans length in special cases. We also indicate how the MSDC of SFRs is expected to evolve with time. Based on these results, we reconsider the Taurus-Auriga, Ophiuchus, and Orion Trapezium star-forming regions in Section 4. Finally, we present our conclusions in Section 5.

## 2 THE MEAN SURFACE DENSITY OF COMPANIONS

In the simplest case, the mean surface density of companions can be determined as follows. For each star, calculate the angular separation  $\theta$  to all other stars. Bin the separations resulting from these stellar pairs into annuli of separation  $\theta$  to  $\theta + \delta\theta$ . The binning is most conveniently done using

annuli with logarithmically increasing radii. The number of separations from such pairs,  $N_p$ , within each size of annulus is then divided by the area of the annulus and averaged by dividing by the total number of stars  $N_*$  giving the mean surface density of companions as a function of separation,  $\Sigma_{\text{com}}(\theta) = N_p/(2\pi \theta \delta\theta N_*)$ . We will refer to this as Method 1. The MSDC is related to the angular two-point correlation function,  $w(\theta)$ , by  $\Sigma_{\text{com}}(\theta) = (N_*/A)(1 + w(\theta))$ , where  $A$  is the survey area (Peebles 1980).

## 2.1 Handling boundaries

For a survey region of finite size, using the above method (Method 1), to calculate  $\Sigma_{\text{com}}(\theta)$ , results in some of the companions to stars closer than  $\theta$  to a boundary being missed. This has little effect if the survey region is large in comparison to  $\theta$ , since only a small fraction of the stars are affected. However, when  $\theta$  becomes large, the missing companions result in an unphysical drop in  $\Sigma_{\text{com}}(\theta)$ .

Several methods for avoiding such boundary effects have been used (see Peebles 1980, and references within). One method is to select an inner subsample of  $N_1$  stars such that none is closer than  $\theta_{\text{max}}$  from a boundary and for each of them calculate the number of companions from the full sample.  $\Sigma_{\text{com}}(\theta)$  is then normalised by dividing by  $N_1$  rather than  $N_*$ . This method (Method 2) avoids boundary effects, but also eliminates some information and does not probe the full range of separations.

A modification of Method 2 (Method 3) is to select a different inner subsample for each size of annulus,  $\theta_i$  to  $\theta_i + \delta\theta$ , such that each subsample of  $N_i$  stars are all farther than  $\theta_i + \delta\theta$  from a boundary. This allows the maximum information to be used for each separation, but again the full range of separations cannot be studied since as  $\theta_i$  increases,  $N_i$  decreases.

Other methods try to correct for the presence of boundaries. In Method 4, the area of each annulus is directly computed for each star (subtracting that part which falls outside a boundary) to give a corrected surface density of companions for that star before the mean over all stars is calculated. Rather than calculate the area of each annulus explicitly (which can be difficult), a similar method (Method 5) calculates a Monte Carlo estimate of the area of each annulus that lies within the survey boundaries. This is achieved as follows:  $N_t$  points are placed at random in the survey area,  $A$ ;  $\Sigma_{\text{com}}(\theta)$  is calculated using Method 1 for both the trial points ( $\Sigma_{\text{trial}}$ ) and for the real data ( $\Sigma_{\text{data}}$ ); then the corrected  $\Sigma_{\text{com}}(\theta)$  of the real data is given by

$$\Sigma_{\text{corr}}(\theta) = \frac{\Sigma_{\text{data}}(\theta)}{\Sigma_{\text{trial}}(\theta)} \frac{N_t}{A}. \quad (1)$$

Methods 4 and 5 correct for boundaries if the distribution of sources on scales of order the survey size is uniform (hence their use in studying the large-scale structure of the universe). However, if there is a surface density gradient across the boundary these methods *do not* fully correct for boundaries, as demonstrated in Section 2.3.

## 2.2 Binaries

Larson (1995) found that the binary systems in Taurus-Auriga are characterised by an MSDC with a power-law

slope of  $\approx -2$ , which can be easily shown to be equivalent to the distribution of binary separations being uniform in the logarithm of separation. Take  $N$  binary systems with separations,  $r$ , distributed as

$$\frac{dN}{d(\log(r))} = k, \quad (2)$$

where  $k$  is a constant. Then

$$dN = \frac{k}{r} dr, \quad (3)$$

is the number of companions with separations in the range  $r$  to  $r + dr$ . Taking a two-dimensional projection, the range  $r$  to  $r + dr$  defines an annulus of area  $2\pi r dr$ . Therefore, the MSDC is

$$\Sigma_{\text{com}}(r) = \frac{1}{N} \frac{dN}{2\pi r dr} = \frac{1}{N} \frac{k}{2\pi r^2}, \quad (4)$$

which has a power-law slope of  $-2$ . Integrating equation 3 to find  $k$  gives

$$\Sigma_{\text{com}}(r) = \frac{1}{2\pi \ln[R_{\text{max}}/R_{\text{min}}] r^2}, \quad (5)$$

where  $R_{\text{max}}$  and  $R_{\text{min}}$  are the maximum and minimum binary separations, respectively. Finally, if not all systems are binaries

$$\Sigma_{\text{com}}(r) = \frac{B_{\text{freq}}}{2\pi \ln[R_{\text{max}}/R_{\text{min}}] r^2}, \quad (6)$$

where  $B_{\text{freq}}$  is the binary frequency (defined as the number of binary systems over the total number of systems).

Thus, Larson's (1995) result for the Taurus-Auriga pre-main-sequence binaries is in general agreement with the period distribution for the main-sequence G-dwarf primaries of Duquennoy & Mayor (1991) which, in the logarithm of period, is flat to first order.

Finally, we note that fitting power-law slopes to the MSDC and comparing the values of the indices is not the best way to compare the distribution of binary separations between star-forming regions since it ignores any deviations from a power-law. Instead, it is preferable to take the usual approach, namely comparing the fractional number of binaries (the number of binaries in a range of separations over the total number of systems) as a function of the logarithm of separation.

## 2.3 Global density profiles

The MSDC for stars distributed uniformly is independent of separation and simply equal to the mean surface density of stars over the whole survey region. If the stars are clustered (Section 2.4) or distributed in a non-uniform, self-similar (fractal) distribution, the MSDC is a function of separation (e.g. Larson 1995). However, a particular MSDC does not correspond to a unique two-dimensional distribution of stars. In particular, an MSDC which has a power-law dependence on separation does not necessarily correspond to a self-similar or fractal distribution of stars; a simpler surface density distribution (e.g. a centrally-condensed density profile) can give the same slope over a large separation range.

In this section, we consider the MSDC of global density profiles. We also study the effects that the different ways of handling boundaries (Section 2.1) have on the MSDC when the underlying density profile is not uniform.

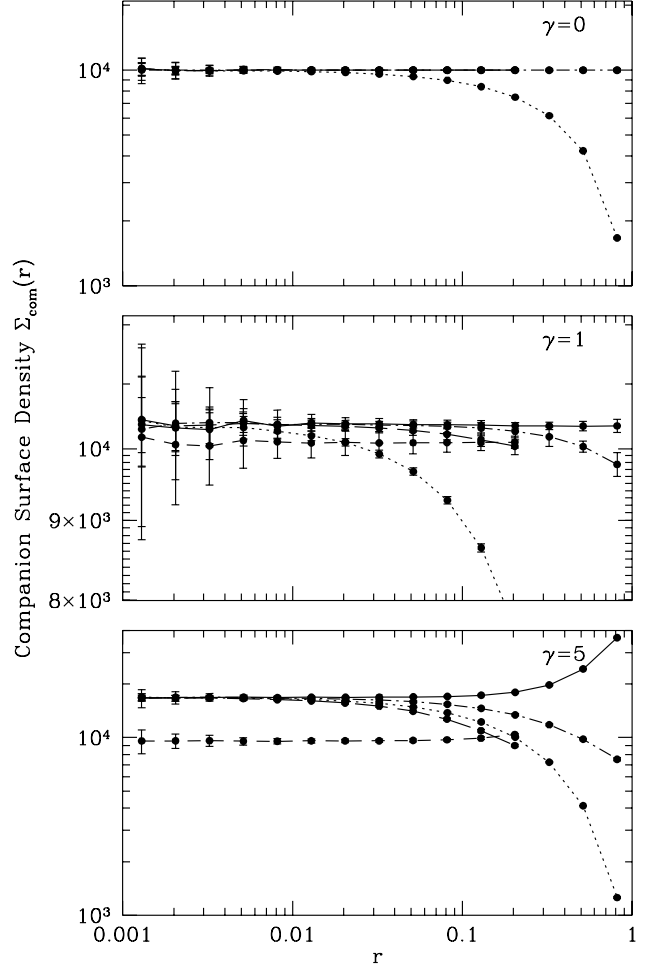


**Figure 1.** The mean surface density of companions  $\Sigma_{\text{com}}(r)$  for four different distributions of  $10^4$  single stars (shown above). The distributions have stellar surface densities  $\Sigma(x) \propto x^\gamma$  with  $\gamma = 0$  (top left, solid line);  $\gamma = 1$  (top right, dotted line);  $\gamma = 2$  (lower left, dashed line); and  $\gamma = 5$  (lower right, long-dashed line). To avoid boundary effects the distributions are continued outside the illustrated area. In each case,  $\Sigma_{\text{com}}(r)$  and its dispersion are calculated from 20–100 random renderings of the distributions.

### 2.3.1 Density gradients

Consider a stellar distribution with a gradient in surface density along one direction  $\Sigma(x) \propto x^\gamma$  with  $x > 0$ . Now, consider the surface density of companions in an annulus of radius  $r_{\text{ann}}$  and width  $\delta r$  centred on one star in the distribution with an  $x$ -coordinate of  $x_*$ . To first order, the surface density at  $x_* + \delta x$  differs from the surface density at  $x_*$  by  $1 + \gamma \delta x / x_*$ . Thus, as long as  $r_{\text{ann}} \ll x_*$ , the mean surface density around the annulus,  $\Sigma_{\text{ann}}(x_*)$ , is approximately equal to the surface density at  $x_*$ ,  $\Sigma(x_*)$ , since the first-order term cancels and only leaves second-order and higher effects: for  $\gamma = 0$  or  $\gamma = 1$  the equality is exact. If each star in the distribution satisfies  $r_{\text{ann}} \ll x_*$ , the MSDC should be almost independent of separation. For  $\gamma = 0$  the value is simply the mean density in the survey area. However, for  $\gamma \neq 0$  the value is greater since the surface density distribu-

**Figure 2.** The mean surface density of companions  $\Sigma_{\text{com}}(r)$  for the distributions from Figure 1 with  $\gamma = 0, 1$ , and  $5$ , but comparing the results from Methods 1 (dotted lines), 2 (dashed lines), 3 (long-dashed lines), and 5 (dot-dashed lines) to the MSDCs without boundary effects from Figure 1 (solid lines).

tion is sampled more in the high-density regions and less in the low-density regions (the sampling points are at the stellar positions) and, hence, a *surface-density-weighted* mean surface density is obtained.

The MSDC for distributions with  $\gamma = 0, 1, 2$ , and  $5$  in Figure 1 demonstrate the lack of dependence of the MSDC on separation for such density gradients and the higher overall values for  $\gamma \neq 0$ . The increase at large radii for  $\gamma = 2$  and  $\gamma = 5$  is due to the second-order and higher effects which become important when  $r_{\text{ann}}$  is of order the survey area's dimensions. Note that in these figures, and all similar ones in this paper, the errorbars are determined by randomly producing 20–100 distributions of stars that follow the prescribed surface density distribution and calculating the mean and standard deviation of the MSDC at each separation.

The MSDC functions in Figure 1 were produced using Method 1 in Section 2.1, but the stellar distributions were continued outside of the regions shown in Figure 1 to avoid

stellar distribution when  $\gamma \neq 0$ . As for  $\gamma = 0$ , using Method 1 results in a rapid drop in the MSDC as the separation increases. Method 2 gives the correct MSDC, but over a smaller region than the whole survey area. With  $\gamma \neq 0$ , this results in a different normalisation because the mean surface density over the smaller area is different to that over the whole survey area. Method 3 gives the correct normalisation on small-scales, but still results in a rapid fall-off at large scales which may even exceed that of Method 1 (e.g. in the case where  $\gamma = 5$ ). Method 5 gives the correct normalisation on small-scales and partially corrects for the fall-off at large separations.

Finally, although none of the methods correct perfectly for the survey boundaries when  $\gamma \neq 0$ , all except Method 1 give a good approximation (i.e. an error of  $\lesssim 0.1$  dex) to the ‘correct’ MSDC if  $0 \leq \gamma \lesssim 2$ .

### 2.3.2 Centrally-condensed stellar distributions

**Figure 3.** Diagram showing the sampling regions of small and large annuli centred on a star a distance  $r_*$  (solid line) from the centre of the global density maximum of a stellar distribution with the radial surface density profile  $\Sigma_r \propto r^{-1}$ . The annuli of radii  $r_{\text{ann}}$  (dashed lines) have width  $\delta r$ . Notice that the mean surface density around the small annulus is approximately equal to the surface density at  $r_*$  ( $\Sigma_{\text{ann}}(r_*) \approx \Sigma_r(r_*)$ ), while the surface density around the large annulus is always less than that at  $r_*$  and, thus, so is the mean ( $\Sigma_{\text{ann}}(r_*) < \Sigma_r(r_*)$ ). In the limit that  $r_{\text{ann}} \gg r_*$ ,  $\Sigma_{\text{ann}}(r_*)$  tends towards  $\Sigma_r(r_{\text{ann}})$ .

missing neighbours at the edges. However, for a real stellar survey, there is no knowledge of the stellar distribution outside of the survey boundaries. Therefore, in Figure 2, we give the MSDC using only the 10000 stars in the area  $1 \leq x \leq 2$  and  $0 \leq y \leq 1$ , calculated using Methods 1, 2, 3, and 5. Since Methods 2 and 3 only use subsets of the data they are only calculated to separations of 1/5 of the survey area’s size as this gives a good trade-off between the range of separations that are covered and the number of stars used for the calculation. Method 4 is not used here since it gives a similar result to Method 5, but is much more difficult to calculate for a simple survey area let alone for an irregular one, since the area of the part of each annulus that falls within the boundaries has to be determined. Throughout this paper, Method 5 is calculated using 10000 trial points in the survey area.

For the uniform density case ( $\gamma = 0$ ), all methods, except Method 1, return the ‘correct’ MSDC (i.e. that given by extending the stellar distribution outside the boundaries of the survey region). Method 1, in which there is no attempt to correct for the effect of the boundaries, gives an MSDC which differs appreciably from the correct MSDC even on scales less than a order of magnitude smaller than the size of the survey region. In particular, if a power-law slope is fit to the MSDC even between such small separations as 1/100 to 1/10 of the survey’s dimensions, a slope of  $-0.055 \pm 0.003$  is derived, rather than a slope of zero.

Due to the density gradients across the boundaries, none of the methods give the ‘correct’ MSDC for the whole

Next, we consider a system of stars distributed according to the radial surface density distribution  $\Sigma_r(r) \propto r^{-\alpha}$  with  $\alpha \geq 0$ . Consider the mean surface density of stars in an annulus of radius  $r_{\text{ann}}$  centred on one star in this distribution with distance  $r_*$  from the position of peak surface density (Figure 3). If  $r_{\text{ann}} \ll r_*$ , the mean surface density of stars in the annulus,  $\Sigma_{\text{ann}}(r_*)$ , is approximately equal to the local surface density  $\Sigma_r(r_*)$ . On the other hand, if  $r_{\text{ann}} \gg r_*$ , the mean surface density of stars in the annulus is less than  $\Sigma_r(r_*)$  and tends towards  $\Sigma_r(r_{\text{ann}})$  (see Figure 3).

Now, consider the *mean* surface density of companions over *all* stars  $\Sigma_{\text{com}}(r_{\text{ann}})$  in a survey region that is centred on the peak surface density. The variation of the MSDC as a function of separation depends on the fraction of the stars that have  $r_{\text{ann}} \gtrsim r_*$ . This fraction increases as  $r_{\text{ann}}$  is increased, but it also depends on  $\alpha$ . For example, for  $\alpha = 1$ , the number of stars within  $r_{\text{ann}}$  of the central peak (i.e. with  $r_* < r_{\text{ann}}$ ) increases linearly with  $r_{\text{ann}}$ . Thus, for larger annuli, more and more stars have  $\Sigma_{\text{ann}}(r_*) < \Sigma_r(r_*)$  but, only when  $r_{\text{ann}}$  is greater than half the radius of the survey area,  $R_{\text{sur}}$ , do less than 50% of the stars have  $\Sigma_{\text{ann}}(r_*) \approx \Sigma_r(r_*)$ . When  $r_{\text{ann}} > R_{\text{sur}}/2$ , most of the stars tend towards  $\Sigma_{\text{ann}}(r_*) < \Sigma_r(r_{\text{ann}})$ . Thus, the MSDC should only decrease slowly as the separation increases, due to the slowly changing number of stars with  $r_* < r_{\text{ann}}$  until  $r_{\text{ann}}$  approaches  $R_{\text{sur}}$  at which stage there is a transition from the slowly decreasing slope to power-law slope of  $-\alpha$ .

For  $\alpha < 1$ , the number of stars that have  $r_* < r_{\text{ann}}$  increases even more slowly with increasing  $r_{\text{ann}}$ . Also, since the radial surface density varies less overall,  $\Sigma_{\text{ann}}(r_*)$  is closer to  $\Sigma_r(r_*)$  even when  $r_* < r_{\text{ann}}$ . Thus, the MSDC depends less on separation. The extreme case is for  $\alpha = 0$  when, since  $\Sigma_r(r_*)$  is constant,  $\Sigma_{\text{ann}}(r_*)$  is always equal to  $\Sigma_r(r_*)$  and so the MSDC is constant.

For  $\alpha > 1$ , however, the number of stars with  $r_* < r_{\text{ann}}$  increases quicker with increasing  $r_{\text{ann}}$  and the overall variation of the radial surface density is more extreme, thus, the MSDC,  $\Sigma_{\text{com}}(r_{\text{ann}})$ , falls faster with increasing  $r_{\text{ann}}$ . In the limit that  $\alpha \rightarrow \infty$ , all the stars are in the central peak and for all stars  $\Sigma_{\text{ann}}(r_*) = \Sigma_r(r_{\text{ann}}) \propto r_{\text{ann}}^{-\alpha}$  so that the MSDC has a power-law slope of  $-\alpha$  for all separations ( $\Sigma_{\text{com}}(r_{\text{ann}}) \propto r_{\text{ann}}^{-\alpha}$ ).

In summary, the MSDC of a uniform distribution of

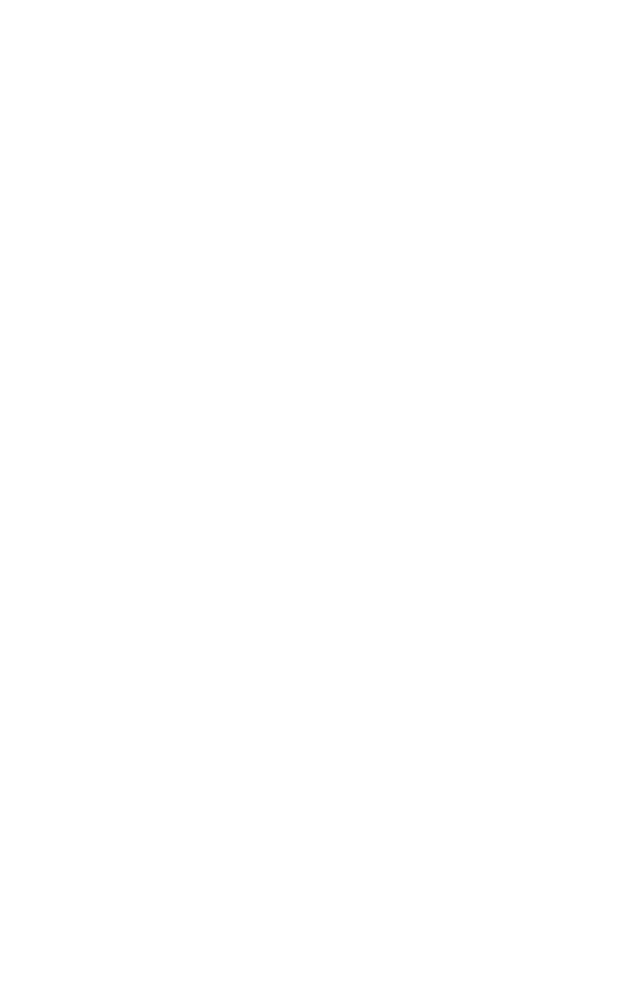


**Figure 4.** The mean surface density of companions  $\Sigma_{\text{com}}(r)$  for four different distributions of  $10^4$  single stars (shown above). The four distributions have radial surface density profiles given by: a)  $\Sigma_r = \text{constant}$  (top left, solid line), b)  $\Sigma_r \propto r^{-1/2}$  (top right, dotted line), c)  $\Sigma_r \propto r^{-1}$  (lower left, short-dashed line), d)  $\Sigma_r \propto r^{-3/2}$  (lower right, long-dashed line). Global surface density profiles less extreme than  $\Sigma_r \propto r^{-1}$  result in essentially flat MSDC functions.

stars is independent of separation, while in the limit  $\alpha \rightarrow \infty$ , the MSDC has a power-law of slope  $-\alpha$ . For intermediate cases, the slope over most separations is less than  $-\alpha$  with a transition towards a slope of  $-\alpha$  when  $r_{\text{ann}} \approx R_{\text{sur}}$ .

In Figure 4, we give the MSDC for global density profiles  $\Sigma_r(r) \propto r^{-\alpha}$  where  $\alpha = 0, 1/2, 1$ , and  $3/2$ . For separations less than  $1/10$  of the dimension of the survey region the MSDC have slopes of  $0, -0.013 \pm 0.004, -0.22 \pm 0.01$ , and  $-1.01 \pm 0.01$ , respectively. This is in agreement with the above analysis (i.e. the slopes are shallower than  $-\alpha$  if  $\alpha > 0$ ). It is important to notice that the *MSDC can have a power-law slope even without any sub-clustering or hierarchical structure* (e.g. see the Jones & Walker MSDC for the Orion Trapezium Cluster in Section 4.3 and Figure 18). As predicted above, the slope deviates from a power-law only for separations  $\gtrsim 1/10$  the survey region size (i.e. when  $r_{\text{ann}} \approx R_{\text{sur}}$ ), when there is a transition towards a slope of

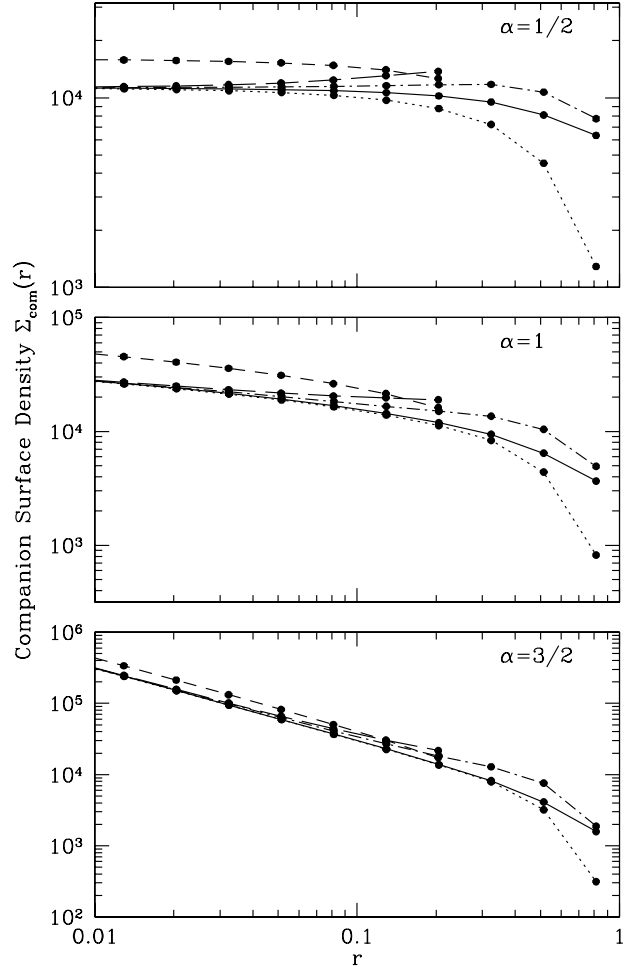


**Figure 5.** The mean surface density of companions  $\Sigma_{\text{com}}(r)$  for the distributions from Figure 4 with  $\alpha = 1/2, 1$ , and  $3/2$ , but comparing the results from Methods 1 (dotted lines), 2 (dashed lines), 3 (long-dashed lines), and 5 (dot-dashed lines) to the MSDCs without boundary effects from Figure 4 (solid lines). In none of the cases do methods 1–5 give perfect correction for boundary effects.

$-\alpha$ . The maximum difference between the small-scale and large-scale power-law slopes occurs for  $\alpha \approx 1$ .

Although all centrally-condensed global density profiles show power-law slopes in the derived MSDC, for  $\alpha \lesssim 1$  the MSDC is rather flat, depending only weakly on separation. This is important because most young clusters are likely to be less centrally condensed than the  $\alpha = 1$  case (e.g. McCaughrean & Stauffer 1994), which corresponds to a three-dimensional density distribution of  $\rho(r) \propto r^{-2}$ , the singular isothermal sphere. Therefore, if a cluster has an overall radial surface density profile and *also* contains sub-clustering and/or hierarchical structure, the sub-structure will generally be detectable because it will steepen the slope of the MSDC and/or perturb it from a true power-law (e.g. Section 4.3.1). Thus, *the MSDC can still be used to look for sub-clustering and/or hierarchical structure even where an overall global density distribution exists*.

As in Section 2.3.1, a centrally-condensed global den-

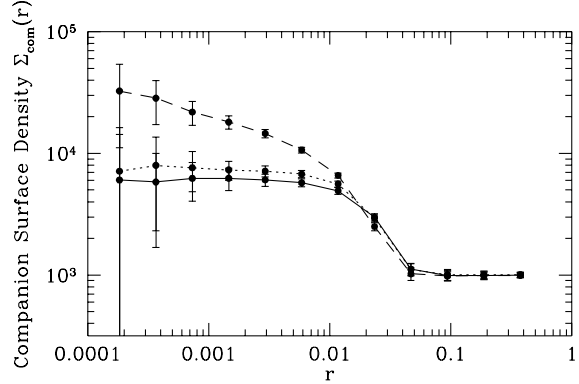


**Figure 6.** The mean surface density of companions  $\Sigma_{\text{com}}(r)$  for three different distributions of clusters of stars (shown above). Each cluster consists of 10 stars distributed uniformly within a sphere of radius 0.025. The three distributions consist of: a) 10 clusters (left, solid line), b) 100 clusters (centre, dotted line), c) 1000 clusters (right, dashed line). The clusters are randomly distributed. Cases b) and c) can be thought of as having the same volume density of clusters as case a), but being 10 and 100 times deeper, respectively. The higher the mean density of stars, the more difficult it is to detect the clustering.

sity profile means that the boundaries of the survey regions are difficult to correct for (Figure 5). Again, Method 1 results in a fall-off for large separations and Method 2 gives a different normalisation (as well as some information being lost). Method 3 over-corrects for the fall-off at large separations. Both Methods 4 and 5 assume that the surface density of companions around an annulus is constant. With a falling global density profile, these methods result in an over-estimate of the mean surface density of an annulus, since the low-density region of the annulus is missing. This results in an over-correction for the MSDC. Finally, note that in calculating the slope of the MSDC for separations  $\gtrsim 1/10$  of the survey's smallest dimension, the relative error decreases as  $\alpha$  increases (c.f.  $\alpha = 1/2$  and  $\alpha = 3/2$ ).

## 2.4 Clusters

Gomez et al. (1993) found that stars in the Taurus-Auriga SFR are not distributed randomly, but instead are clustered into small groups. It is therefore of interest to consider the MSDC of clusters of stars. Examples of the MSDC derived for randomly-distributed simulated clusters are given in Figure 6. They are characterised by an MSDC equal to the global mean surface density on large scales, but have larger than average surface densities on small scales with a transition between the two regimes for separations of order the clusters' radii.

On scales less than the cluster radius, the MSDC depends on the spatial distribution of stars within the clus-

**Figure 7.** The mean surface density of companions  $\Sigma_{\text{com}}(r)$  for three different distributions of clusters of stars. In each case, the distributions consist of 100 randomly-positioned clusters of 10 stars (i.e. as in case b) in Figure 6). The clusters have radii of 0.025 and the distributions of stars within the clusters are given by: a)  $\rho = \text{constant}$  (solid line), b)  $\rho \propto r^{-1}$  (dotted line), and c)  $\rho \propto r^{-2}$  (dashed line).

ters. Clusters with uniform volume density (Figure 6) give a flat MSDC on small scales, while centrally-condensed clusters give an MSDC that rises as the separation is decreased (Figure 7). This is analogous to the power-law slopes of the MSDCs that result from the centrally-condensed global density profiles in Section 2.3.2. However, the clusters have to be quite centrally condensed for there to be much effect. Clusters with density profiles of  $\rho \propto r^{-2}$  have power-law slopes of  $-0.22 \pm 0.01$  on small scales (as determined in Section 2.3.2), but clusters with  $\rho \propto r^{-1}$  still give an essentially flat MSDC. Therefore, it is difficult to determine whether or not clusters are centrally condensed unless they have density profiles of  $\rho \propto r^{-2}$  or steeper (i.e.  $\Sigma_r(r) \propto r^{-1}$ ).

Given a distribution of stars, it is important to be able to detect whether the stars are clustered. The sensitivity of the MSDC to clustering depends on the crowding of the clusters and on the fraction of stars that are not members of clusters. Figure 6 demonstrates that the more crowded clusters are, the more difficult it becomes to detect them. Well-separated clusters are detectable because the mean surface density of companions on small scales (within a cluster) is larger than the global mean surface density. If the global mean surface density of companions within a cluster, the confusion limit is reached; the clusters overlap and it is no longer possible to distinguish that the stars are clustered. The confusion limit can be approached either because the clusters actually overlap, or because a three-dimensional distribution of clusters is projected on to the two-dimensional plane of the sky. The rate at which the confusion limit is reached with increasing depth depends on the volume-filling factor; if the clusters are well-separated in three-dimensions, a larger depth is required before the clusters begin to overlap. The detection of binaries (effectively very simple clusters) suffers from the same effect (see Section 3.1).

A similar effect can be obtained by including unclustered stars (Figure 8). Even if clusters are well-separated on the sky, stars that are not cluster members (e.g. randomly-



**Figure 8.** The mean surface density of companions  $\Sigma_{\text{com}}(r)$  for four different distributions of  $10^3$  single stars (shown above). The four distributions differ in the fraction of stars that are in clusters: a) 100% (top left, solid line), b) 70% (top right, dotted line), c) 30% (lower left, short-dashed line), d) 10% (lower right, long-dashed line). Each cluster consists of 10 stars distributed uniformly within a sphere of radius 0.025. The lower the fraction of stars that are in clusters, the more difficult the presence of clusters is to detect.

distributed stars) decrease the difference between the mean surface density of companions on small and large scales. Unclustered stars have a low companion surface densities on small scales. Thus, the more unclustered stars there are, the lower the *mean* surface density of companions becomes on small scales and the closer it becomes to the global mean surface density. In Figure 8 one can easily detect when 30 – 100% of the stars are in clusters, but the detection when 10% of the stars are in clusters is only a  $\approx 3\sigma$  result at separations close to the radii of the clusters with an even a less significant detection at smaller separations.

## 2.5 Self-similar distributions

Larson (1995) found that the MSDC of the stars in the Taurus-Auriga SFR could be well fit by a power-law slope of  $\approx -0.6$  on large scales ( $\gtrsim 0.04$  pc). In general, the number of stars within an angular distance  $\theta$ , on the sky, of an average star increases as  $\theta^{(\text{slope}+2)}$ . For a fractal point distribution with fractal dimension  $F_{\text{dim}} \leq 2$ , the number of stars closer

than  $\theta$  increases as  $\theta^{F_{\text{dim}}}$ . Thus, Larson noted that the large-scale distribution of stars in the Taurus-Auriga SFR could be described as a fractal point distribution with fractal dimension  $F_{\text{dim}} = \text{slope} + 2 \approx 1.4$ .

In this section we consider the MSDC of self-similar (or fractal) stellar distributions. Figure 9 gives the MSDCs for stellar distributions with fractal dimensions of  $F_{\text{dim}} = 1.4$ , 1.9, and 2.4. The distributions were produced using a box-counting algorithm: a cube of side-length  $L$  is divided into  $N_{\text{div}}^3$  sub-cubes of side-length  $L/N_{\text{div}}$ ;  $N_{\text{ran}}$  of these sub-cubes are randomly selected; the process is repeated recursively, terminating at the desired level of recursion when each of the smallest sub-cubes has a star placed in it. The fractal dimension is given by  $F_{\text{dim}} = \log_e(N_{\text{ran}})/\log_e(N_{\text{div}})$ . To obtain a specific number of stars, some of the stars are randomly selected and removed. To get a rectangular volume that has one dimension longer than the other two, a fractal distribution is created for a cube of the largest dimension, and the desired rectangular volume is given by a sub-volume of the cube.

For each fractal dimension, we examine the dependence of the MSDC on the effects of the depth of the stellar distributions. In Section 2.4 and Figure 6, we found that it becomes more difficult to detect clustering as the clusters become more crowded on the sky. If clusters are distributed randomly in three dimensions, then looking through 10 times the depth, raises the MSDC on large scales by an order of magnitude and decreases the difference between the MSDC on small and large scales.

With fractal stellar distributions, the effect of the depth of the SFR depends on the fractal dimension (or volume-filling nature) of the stellar distribution. Some examples are as follows. A random (or uniform) point distribution in three dimensions has a fractal dimension  $F_{\text{dim}} = 3$ , since the number of companions within a distance  $r$  of a typical star increases as  $r^3$ . A uniform two-dimensional distribution has a fractal dimension  $F_{\text{dim}} = 2$ , while a uniform linear distribution has  $F_{\text{dim}} = 1$ , and a single point has a fractal dimension of  $F_{\text{dim}} = 0$ . Other distributions with the same fractal dimensions as those above are possible (except for  $F_{\text{dim}} = 0$ ). For a uniform three-dimensional stellar distribution ( $F_{\text{dim}} = 3$ ), if the depth is increased by an order of magnitude, then the MSDC is also increased by an order of magnitude independent of separation (e.g. Figures 6 and 10). However, in general, for a three-dimensional stellar distribution with  $F_{\text{dim}} < 3$ , the MSDC increases by *less* than one order of magnitude if the depth is increased by one order of magnitude, since the number of companions does not increase linearly with depth. In general, the MSDC is increased (on the largest scales) by

$$\text{MSDC} \propto D^{F_{\text{dim}}/3}, \quad (7)$$

where  $D$  is the depth. In the limit that  $F_{\text{dim}} = 0$ , there is only ever one object no matter what factor the depth is increased by. Note however, that the dependence of the MSDC on depth depends somewhat on the specific distribution and/or orientation. For example, in the case of a uniform linear distribution, if the depth increases parallel to the line of objects, then the MSDC will increase linearly with depth, while if the depth increases perpendicular to the line of objects, increasing the depth will have no effect on the MSDC. In general (i.e. when all possible distributions

**Figure 9.** The mean surface density of companions  $\Sigma_{\text{com}}(r)$  for three different self-similar (fractal) stellar distributions. The three distributions have fractal dimensions a)  $F_{\text{dim}} = 1.4$  (left), b)  $F_{\text{dim}} = 1.9$  (centre), c)  $F_{\text{dim}} = 2.4$  (right). For each case,  $\Sigma_{\text{com}}(r)$  is given for stellar distributions with depths of 1 (solid line and upper left graph), 10 (dotted line and upper right graph), and 100 (dashed line and lower left graph) times the horizontal or vertical dimension of the survey region. Examples of the stellar distributions are given above the graphs of  $\Sigma_{\text{com}}(r)$ , with the lower right graphs giving the distribution of stars in the  $z$  (depth) dimension. Notice that for higher  $F_{\text{dim}}$  the stars become more uniformly distributed with depth. Also, with a low  $F_{\text{dim}}$ , as the depth is increased the number of stars is increased, but the additional stars typically do not appear in regions already occupied by closer stars. Thus, the MSDC on small-scales is relatively independent of the depth for low fractal dimensions.

are averaged over), however, the MSDC follows equation 7 on the largest scales.

The scaling of equation 7 is apparent in Figure 9; in general, on the largest scales, increasing the depth has a greater effect on the MSDC for distributions with greater fractal dimensions (greater volume-filling factor). However, note that increasing the depth affects the MSDC on large scales more than on small scales and this effect is more apparent for lower fractal dimensions. To use an analogy from the clusters in Section 2.4, larger structures begin overlapping before smaller structures, with the result that, *for fractal dimensions  $F_{\text{dim}} < 3$ , the MSDC is more sensitive to the depth of a SFR on large scales than on small scales*. In particular, for a fractal dimension of  $F_{\text{dim}} = 1.4$ , the MSDC on scales less than  $\approx 1/25$  of the survey region's dimensions varies by less than a factor of 2 even if the depth is increased by a factor of 100.

### 3 THE BREAK BETWEEN THE BINARY AND LARGE-SCALE REGIMES

Larson (1995) demonstrated that there is a break in the slope of the MSDC for the Taurus-Auriga SFR, and Simon (1997) found similar breaks in the MSDCs of the Ophiuchus and Orion Trapezium regions. Larson identified the break as being at the length scale where the MSDC goes from being dominated by binaries to being dominated by large-scale structure (e.g. clustering or self-similar structure). The fact that a break occurs indicates that a single scale-free

process is not responsible for the formation of both binaries and large scale clustering. Larson also noted that the break occurred at a length scale roughly equal to the typical Jeans length in the Taurus-Auriga SFR and speculated that this was evidence that, for length scales less than the Jeans length, binaries are formed via fragmentation of a single collapsing cloud core while, on larger scales, stars are distributed self-similarly. However, Simon (1997) found that the breaks between the binary and large scale regimes occur at smaller separations in star-forming regions with higher stellar densities. Furthermore, in the SFRs considered by Nakajima et al. (1998), the location of break varied from  $\approx 1000 - 30000$  AU.

In this section we consider the origin of the break between the binary and large-scale regimes in the MSDC. First, we investigate what determines the break in SFRs with a uniform stellar distribution. We then consider the behaviour of the transition separation in regions where the stars are clustered or distributed self-similarly. Finally, we predict how the location of the break varies as a SFR evolves with time due to expansion and/or the erasing of initial self-similar structure.

#### 3.1 Uniform stellar distributions

Consider  $N$  stellar systems with a uniform spatial distribution in a volume with dimensions on the sky of  $X$ ,  $Y$ , and depth  $Z$ . Those systems that are binaries have separations distributed as in equation 2. On large scales the MSDC is simply the mean surface density of stars



**Figure 10.** The mean surface density of companions  $\Sigma_{\text{com}}(r)$  for three distributions stellar systems (shown above). In all cases, each stellar system is a binary system with separation in the range 0.1 to  $10^4$  AU, and the mean three-dimensional distance between the stars is the same ( $d_3 = 0.28$  pc =  $5.7 \times 10^4$  AU, dotted vertical line), but the depth of the volume varies: a) 0.28 pc (top left, and solid line), b) 2.8 pc (top middle, and dotted line), and c) 28 pc (top right, and dashed line). The break between the binary and large-scale regimes moves to smaller separations simply because the projected surface density of stars increases.

$$\Sigma_{\text{mean}} = \frac{N(1 + B_{\text{freq}})}{XY} = \frac{4}{\pi d_2^2}, \quad (8)$$

where  $d_2$  is the mean (two-dimensional) separation of stars on the sky. On small scales most companions are members of the binary systems, so that the MSDC goes as equation 6. The transition between the two occurs at the separation where the two sections of the MSDC are equal (see Figure 10). Equating equations 6 and 8 we find that the break occurs at the separation

$$R_b = d_2 \sqrt{\frac{B_{\text{freq}}}{8 \ln[R_{\text{max}}/R_{\text{min}}]}}. \quad (9)$$

The mean separation between the stars on the sky,  $d_2$ , depends both on the mean volume density of stars

$$\rho = \frac{N(1 + B_{\text{freq}})}{XYZ} = \frac{6}{\pi d_3^3}, \quad (10)$$

where  $d_3$  is the mean three-dimensional distance between stars, and on the depth  $Z$  since

$$\Sigma_{\text{mean}} = \rho Z. \quad (11)$$

Thus, using equations 8 to 11,

$$R_b = d_3 \sqrt{\frac{d_3}{Z}} \sqrt{\frac{B_{\text{freq}}}{12 \ln[R_{\text{max}}/R_{\text{min}}]}}. \quad (12)$$

Hence, the separation at which the break between the binary and large-scale regimes occurs depends on the mean volume density of stars, the depth of the SFR ( $Z/d_3$ ), and, to some

extent, on the parameters of the binaries themselves (the binary frequency  $B_{\text{freq}}$  over the separation range  $R_{\text{min}}$  to  $R_{\text{max}}$ ).

The dependencies of  $R_b$  are demonstrated in Figures 10 and 11. In Figure 10a, 50 binary stellar systems (100 stars) with separations ranging from 0.1 to  $10^4$  AU are placed within a volume with dimension on the sky of 2 pc by 2 pc, and depth  $Z = d_3 = 0.28$  pc (obtained by setting  $Z = d_3$  in equation 10) so that the volume is essentially two-dimensional. In Figures 10b–c, the volume density is kept constant, but the depth is increased by a factor of 10 each time ( $Z = 2.8$  pc and  $Z = 28$  pc respectively). This is also equivalent to keeping  $Z$  fixed, but increasing the volume density by a factor of 10 each time (except this would mean that wide binaries begin to overlap with neighbouring systems). The resulting MSDC for each of Figures 10a–c is given below the stellar distributions. As predicted by equation 12, the position of the break moves to smaller separations with increasing surface density, even though the parameters of the binaries remain unchanged. This explains the finding by Simon (1997) that the position of the break varies between star-forming regions and seems to depend on the stellar density of the region.

Figure 11 shows the effects of changing the parameters of the binaries. Decreasing the binary frequency, but keeping the total number of stars the same moves the break to smaller separations. Keeping the binary frequency constant, but decreasing the range of separations moves the break to larger separations, so long as the maximum binary separation is greater than  $R_b$ . These effects are minor, however, compared to changes in the large-scale surface density.

While Larson (1995) identified the break in the MSDC of the Taurus-Auriga SFR with the typical Jeans length,  $R_{\text{Jeans}}$ , in the molecular cloud, equation 12 shows that the separation at which the break occurs is *not necessarily* equal to the Jeans length. The basis of Larson's argument that the break identifies the Jeans length is that binaries form from the collapse and fragmentation of Jeans-critical cloud cores, while large-scale structure depends on the structure in molecular clouds. From this, one may expect that the maximum binary separation is approximately equal to the size of the cores and, thus, is less than or approximately equal to the mean distance between stars  $d_3$ . However, we found above that the break occurs when a *projected* companion has an equal probability of being a binary or non-binary companion. From equation 12 and Figures 10 and 11, for reasonable binary parameters and  $Z \gtrsim d_3$ , the separation at which the break occurs is *always less* than  $d_3$  by at least an order of magnitude (dotted vertical lines), *regardless* of the Jeans length. Also, binaries may exist with separations  $\gg R_b$  (especially if  $Z > d_3$ ); they are just hidden because the mean surface density of stars in the survey region is greater than the MSDC of binary companions at large separations (i.e. the confusion limit has been reached). Thus, *in general, for a uniform distribution of stellar systems, the break in the MSDC function does not give the Jeans length in a star-forming region*. For  $R_b$  to be similar to the Jeans length, either the star-forming region must be very shallow (i.e.  $Z \lesssim d_3$ ) in which case  $R_b \approx d_3 \approx R_{\text{Jeans}}$ , or  $R_{\text{Jeans}} \ll d_3$  in which case  $R_b$  might approximate the Jeans length because  $R_b \ll d_3$  also.

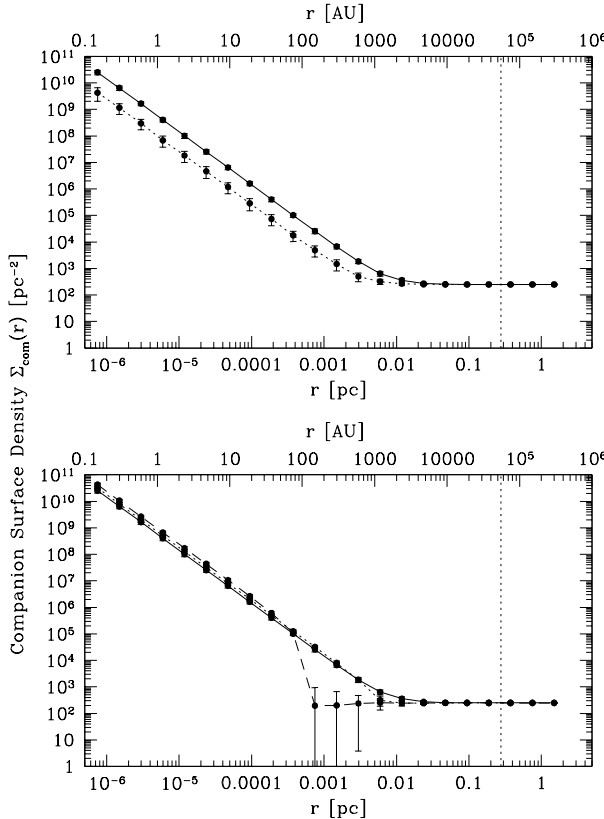


**Figure 11.** The mean surface density of companions  $\Sigma_{\text{com}}(r)$  for stellar systems distributed as in Figure 10b, but with different assumptions about the binaries. In the standard case (solid lines) each stellar system is a binary system with separation in the range 0.1 to  $10^4$  AU. In the upper graph a), we also show the effect if, rather than every system being a binary ( $B_{\text{freq}} = 1.0$ ), only 10 percent of systems are binaries ( $B_{\text{freq}} = 0.1$ ) with the total number of stars being the same (dotted line). In the lower graph b), the binary frequency is always  $B_{\text{freq}} = 1.0$ , but the upper cut-off in the distribution of separations is varied: 10000 AU (solid line), 1000 AU (dotted line), and 100 AU (dashed line). The dotted vertical lines give the mean three-dimensional distance between stars,  $d_3$ . The break between the binary and large-scale regimes moves to smaller separations if the binary frequency is lower, and there is an abrupt drop in the MSDC if the binary separations are truncated at separations less than value of  $R_b$  predicted by equation 12.

### 3.2 Non-uniform stellar distributions

To obtain equation 12, we assumed the stellar systems had a uniform spatial distribution. For non-uniform stellar distributions, the separation at which the transition from the binary to the large-scale regimes occurs has the same dependence on the parameters of the binaries. However, rather than the break occurring when the MSDC of the binaries (equation 6) is equal to the mean surface density of stars (equation 8), the break occurs at the separation where equation 6 is equal to the MSDC of the distribution of stellar systems, which may have its own structure (e.g. Sections 2.3.1, 2.3.2, 2.4, 2.5 and 4.1). If the volume-filling factor of stellar systems is high in the survey volume, the transition separation still depends on the volume density of stellar systems,

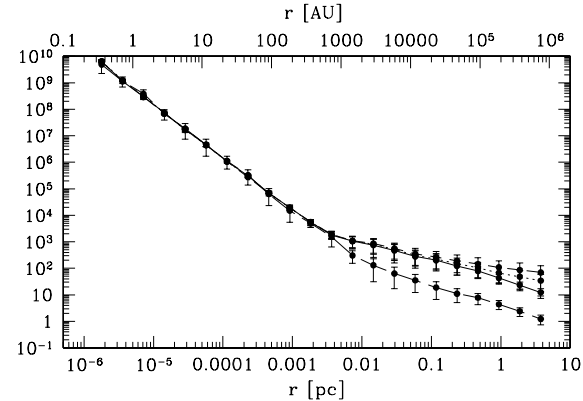


**Figure 12.** The mean surface density of companions  $\Sigma_{\text{com}}(r)$  for stellar systems distributed self-similarly with fractal dimension  $F_{\text{dim}} = 1.4$  (similar to Figure 9a). Each stellar system is a binary system with separation in the range 0.1 to  $10^4$  AU. Four different cases are illustrated. Case a) (solid) has 500 systems (1000 stars) distributed within a region of size  $10 \times 10 \times 10$  pc (i.e. depth = 1). Cases b) and c) are identical, except that the depths are increased to 100 (dotted) and 1000 (short-dashed) pc, respectively. Case d) is identical to the first, except that only 1/10 of the systems are included to mimic incompleteness (long-dashed, lower curve). Note that with  $F_{\text{dim}} = 1.4$ , the depth of the survey region has no effect on the location of the break between the binary and the large-scale regimes, while incomplete surveying of stellar systems results in a shift of the break to larger scales.

and on the depth of the survey volume. However, if the volume filling factor is low the depth of the stellar distribution may be less important. To illustrate this point, we consider the MSDCs both of randomly-distributed clusters of binary stellar systems, and of fractal distributions of binary stellar systems.

Consider a stellar distribution comprised of randomly-distributed clusters of binary stellar systems. The large-scale MSDC is similar to those given in Figure 6, where distributions b) and c) are the same as a) but the depth of the volume is increased by factors of 10 and 100, respectively. Assuming that the MSDC of the binaries equals the MSDC of the systems at a separation less than the radii of the clusters then, even though the depth of the volume is increased by a factor of 10–100, the transition separation is almost unchanged because the system MSDC on scales less than the cluster radius is given by the surface density of stars in the clusters which is unchanged until clusters begin to overlap with each other.

Figure 12 gives the MSDC for fractal distributions of binary stellar systems. In each case, the fractal dimension is  $F_{\text{dim}} = 1.4$ . In cases b) and c) the depth of the region is 10 or 100 times that of case a), respectively. As expected, with such a low fractal dimension, the transition separation is almost independent of the depth (c.f. Figure 9). A variation in the transition separation can be obtained if the number of systems that are included in the calculation of the MSDC is decreased (Figure 12d, which mimics an incomplete survey) or if the dimensions of the survey region are changed but the number of systems is unchanged (i.e. a SFR with a different volume density of stars). The difference between Figures 12a



**Figure 13.** The mean surface density of companions  $\Sigma_{\text{com}}(r)$  for four different distributions of 500 stellar systems (three shown above). Each stellar system is a binary system with separation in the range 0.1 to  $10^4$  AU. In each case, the stellar systems were initially distributed self-similarly with  $F_{\text{dim}} = 1.4$  and the depth of the region is unity. However, these distributions were evolved by moving each system in a random direction by a) 0.01 pc (solid), b) 0.1 pc (dotted line; left), c) 1 pc (short-dashed; centre) and d) 10 pc (long-dashed; right). This mimics the effect of the distribution evolving with time due to a random system velocity dispersion of 1 km/s over  $10^4$ ,  $10^5$ ,  $10^6$  and  $10^7$  years, respectively. Note that the binary and very-large-scale regimes are unchanged, but at intermediate separations  $\Sigma_{\text{com}}(r)$  is flat.

and 12d demonstrates the importance of having a complete stellar survey.

Gomez et al. (1993) interpreted the stellar systems in the Taurus-Auriga SFR as being primarily grouped in small clusters which were well-separated on the sky (see also Section 4.1). Larson (1995) interpreted the systems as being distributed with a fractal dimension  $F_{\text{dim}} = 1.4$ . In either case, the volume-filling factor is low. Therefore, the depth of the SFR is relatively unimportant and the transition separation between the binary and large-scale regimes is determined either by the surface density of the stars within the clusters, or by the projected separation at which binary companions are as common as fractal companions. In the case of the stars being distributed in clusters, when the mean separation of stellar systems is estimated for the stars within these clusters (Section 4.1), the clusters are found to be approximately ‘two-dimensional’, in that the depth of the clusters is approximately equal to the mean separation between systems ( $Z \approx d_3$ ). Therefore, from equation 12, the transition separation will be within an order of magnitude of  $d_3$  and hence similar to the maximum binary separation and presumably to the size of Jeans-critical cloud cores. For the fractal distribution, projection effects are unimportant due to the low fractal dimension and, therefore, the projected separation at which binary companions are as com-

mon as fractal companions is approximately equal to the three-dimensional separation at which binary and fractal companions are equally likely. Thus, as with the clusters interpretation, the transition separation again closely estimates the typical size of Jeans-critical cloud cores. This explains why Larson (1995) obtained good agreement between  $R_b$  and the expected Jeans length in the Taurus-Auriga SFR. In regions such as the Orion Trapezium Cluster, however, this is not the case since the volume-filling factor is high and the SFR is deep (Section 4.3).

### 3.3 Evolution with time

#### 3.3.1 Erasure of substructure

If the stellar distribution in a star-forming region has some structure initially, this structure will slowly be lost as the system evolves due to the stellar velocity dispersion and the evaporation of bound clusters. Structure will be lost on the smallest scales first, with larger scales being affected as the SFR ages. In the long-term, especially for SFRs that are initially unbound, the stars will evolve towards a homogeneous distribution with no structure (i.e. a flat MSDC).

Assuming that self-gravity is unimportant in maintaining initial structure (e.g. unbound associations rather than bound clusters), the effects of time can be mimicked by moving each stellar system (single, binary, or higher-order multiple system), in a random direction, by the mean system velocity dispersion multiplied by the time since the stars formed. In Figure 13, we show how an initially fractal distribution of binary stellar systems evolves with time due to such a velocity dispersion. As predicted, fractal structure on the smallest scales is erased first and the distribution becomes homogeneous on those scales. For an initially fractal distribution, this results in a flat MSDC on scales larger than the binary regime and smaller than the undisturbed fractal regime, with the homogeneous regime extending to larger length scales with time. Eventually, over a finite area, the stars have mixed so much that any initial structure is completely lost (after  $10^7$  years in Figure 13). Note also that the break between the binary and large-scale regimes moves to larger separations with time since the smallest structures (which have the highest stellar density) are disrupted first. When all structure has been erased, the transition separation is simply given by equation 12. Finally, the systems will continue to disperse after all the initial structure has been erased, further lowering the MSDC on large-scales, and thus the transition separation will continue to grow (see also Section 3.3.2).

A similar process occurs with unbound clusters (associations) of stars; the clusters get larger in spatial extent, their stellar density decreases, and hence the break between the binary and large-scale regimes moves to larger separations.

With bound clusters, structure on the smallest scales will again be erased rapidly, and the only remaining structure will be the radial density profile of the overall cluster which, as seen in Section 2.3.2, has a very flat MSDC (a singular isothermal sphere has an MSDC with a power-law slope of  $\approx -0.2$ , and less centrally-condensed configurations are even flatter).

### 3.3.2 Expansion of open clusters

In the above sections, considering the derivation of the position of the break between the binary and large-scale regimes, we have assumed that binaries with separations  $\geq R_b$  exist. Although this is likely in a young star-forming region, it may not always be the case. For example, consider the evolution of an open cluster. When the cluster has just formed, the mean distance between stellar systems is small and wide binaries are prone to being disrupted (e.g. Kroupa 1995a,b,c). Later in the cluster's evolution it expands due to gas loss. This lowers the mean density of stars and hence the break between the binary and large-scale regimes in the MSDC moves to larger separations. However, since wide binaries have been destroyed, the predicted position of the break may exceed the separations of the widest binaries. The result is that the MSDC shows the characteristic slope of  $\approx -2$  for small separations where the binaries exist, but that at the separation beyond which binaries have been destroyed, the MSDC drops abruptly to the mean surface density of stellar systems within the survey region (e.g. Figure 11b). Such absence of wide binaries may be visible in open clusters such as the Pleiades and Hyades. If so, this would give an indirect record of how dense the star clusters were when the stars were initially formed: knowing the widest binaries remaining and assuming a timescale for the expansion of the cluster from its initial density, the stellar density required to destroy wider binaries on a timescale less than the expansion time of the cluster can be determined (see Section 4.3.2; Binney & Tremaine 1987).

Finally, note that for separations larger than that of the widest binary the companions to stars from which the MSDC is calculated are given by chance projections or unbound neighbours. In a survey of a small number of stars it is likely that no such companions exist which results in a gap in the MSDC rather than a drop from the binary regime to the mean surface density of stars (hence the large error-bars for separations just greater than the maximum binary separation in Figure 11b).

## 4 APPLICATION TO STAR-FORMING REGIONS

In the previous sections, we have examined the mean surface density of companions of global density profiles, binaries, clusters, fractals and have determined the dependencies and evolution of the position of the break between the binary and large-scale regimes. We now apply these results to the Taurus-Auriga, Ophiuchus, and Orion Trapezium star-forming regions. Taurus-Auriga has been studied by Larson (1995), while Simon (1997) studied all three regions and Nakajima et al. (1998) studied Ophiuchus and the Orion A, B, and OB star-forming regions. However, in light of the above results, a reanalysis is worthwhile.

### 4.1 Taurus-Auriga

Both Larson (1995) and Simon (1997) determined the MSDC for the Taurus-Auriga SFR. Larson used the sample of 121 sources from Gomez et al. (1993) for the large-scale distribution of stellar systems ( $\theta > 5''$ ) combined with data

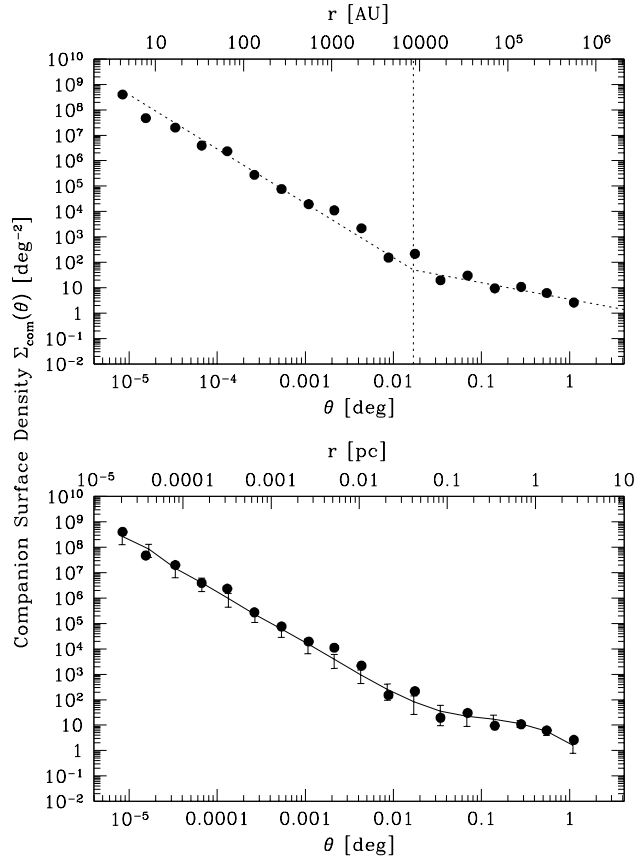


**Figure 14.** The mean surface density of companions  $\Sigma_{\text{com}}(r)$  for the Taurus-Auriga SFR. In the upper graph a), the MSDC derived by Simon (1997) (points) is overlaid on the power-law fit to the MSDC obtained by Larson (1995). In the lower graph b), the MSDC of binary stellar systems distributed in randomly-positioned clusters (see text) is overlaid on the MSDC derived by Simon (1997). Both the broken power-law and cluster-MSDC provide good fits to the data, indicating that the interpretation of the sloping MSDC on large scales being due to fractal structure is not the only interpretation.

from Simon (1992), Ghez et al. (1993), and Leinert et al. (1993) for small separations ( $0.1 \lesssim \theta < 10''$ ). Simon (1997), on the other hand, used a sub-sample of just 49 systems that had been well-surveyed for companions in the separation range 0.005 to  $10''$  resulting in a total of 80 stars (Simon et al. 1995).

This difference in samples is important, since it is relatively meaningless to study the MSDC of an incomplete and/or non-uniformly sampled fraction of the total stellar population of a region. The Gomez et al. (1993) sample was relatively complete to systems with minimum separations  $\approx 5''$ , and as a consequence, they stated in their paper: "... most of the optically visible objects with  $V \lesssim 15.5$  close to the Taurus-Auriga molecular cloud have already been found. ...heavily extinguished infrared sources ... appear to constitute a modest fraction of the total pre-main-sequence population. Therefore it seems worthwhile to begin to investigate the spatial distribution of young stars in Taurus."

Thus, the cumulative sample used by Larson (1995) gives a better determination of the MSDC on the large scales

than the incomplete sub-sample used by Simon (1997), while on the small scales, the two samples are fairly similar, since most of the systems used by Simon were previously known and used by Larson.

Both Larson and Simon found that the large-scale regime can be well fit by a power-law slope of  $\approx -0.6$  (see Figure 14a), which both took to imply a self-similar or fractal distribution. However, we have shown in Section 2 that a given MSDC slope does not correspond to a unique density distribution, and thus it is interesting to ask how robust the result of Larson and Simon is. For example, rather than requiring a self-similar structure to fit the data, could the stars simply be in randomly-distributed clusters?

In Figure 14a, we show the MSDC for Taurus-Auriga derived by Simon (points) with the split power-law fit derived by Larson (dotted line). In Figure 14b, the same MSDC data from Simon are again plotted as points, but the solid line fit is now from a model stellar distribution. We took 40 stellar systems, each composed of a binary distributed in the separation range  $1 - 2 \times 10^4$  AU according to equation 2. Note that since Simon defined two stars to be a binary if their separation was  $\theta < 10'' \approx 1400$  AU, our choice of 40 binary systems with a larger range of separations gives roughly the same numbers of stars (80) and systems (49) that are contained in Simon's sample.

The stellar systems are distributed over the same area as Simon's sample of stars, with 30% randomly distributed, and the remaining 70% in clusters of radius  $R_{\text{clus}} = 2$  pc, each with 8 systems (16 stars) centrally condensed with  $\rho \propto r^{-2}$ . We assume a distance of 140 pc to Taurus-Auriga (Wichmann et al. 1998). Such a distribution is consistent with that determined for the Taurus-Auriga SFR by Gomez et al. (1993) since, although they find clusters consisting of 9–18 stars (with separations greater than  $\approx 5''$ ) with radii 0.5–1.1 pc, the radii depend on the arbitrary stellar surface density at which the cluster is defined to stop. We point out that the mean distance between systems in each cluster is  $\sim 1$  pc, and therefore each cluster is essentially two-dimensional (i.e.  $R_{\text{clus}} \approx Z \approx d_3$ ; see Sections 3.1 and 3.2).

This model MSDC provides an excellent fit to the data points of Simon (Figure 14b) and, moreover, it is not unique, with other randomly-distributed cluster models possible. Thus, while the large-scale structure in Taurus-Auriga is consistent with a fractal structure of dimension 1.4 (Larson 1995; Simon 1997), it is equally consistent with random clustering. To differentiate between the two would require extending the MSDC to larger scales: however, this is not possible, since the data used by Larson already covers the full star-forming region.

Another way to differentiate between the two might be to use higher-order correlation functions than the MSDC (which is equivalent to the two-point correlation function) and/or the nearest-neighbour distribution. The latter has been used by Nakajima et al. (1998) to argue that a MSDC with a power-law slope that is negatively large might indicate a spread of stellar ages rather than stars being formed with a self-similar distribution. They model the Orion B SFR by a mixture of randomly-distributed stars and clusters of different stellar surface densities (the larger of which are assumed to be older than the smaller ones) and obtain a good fit to the MSDC and a better fit to the nearest-neighbour distribution than that implied by a purely fractal

stellar distribution. This is similar to the above demonstration that the Taurus-Auriga MSDC can be modelled using clusters rather than fractal structure (although we use several identical clusters rather than a mixture). However, we point out that the nearest-neighbour distributions found by Nakajima et al. (1998) *do not exclude* the possibility that stars are formed with a self-similar distribution, since the nearest-neighbour and MSDC distributions can be fit by the combination of fractal and homogeneous (presumably older) populations as well as the cluster and homogeneous populations of Nakajima et al.

## 4.2 Ophiuchus

Simon (1997) studied the spatial distribution of 35 stellar systems (51 stars) in the Ophiuchus SFR. He found that on small scales ( $\lesssim 5000$  AU) the MSDC had a power-law slope of  $-1.9 \pm 0.1$  while on large-scales the MSDC could be described by a power-law slope of  $-0.5 \pm 0.2$  (similar to the Taurus-Auriga SFR). Nakajima et al. (1998) studied two samples of stars from the Ophiuchus SFR. The first sample consisted of 86 H $\alpha$  emission line stars (Wilking, Schwartz & Blackwell 1987), 10 of which are known binaries (Reipurth & Zinnecker 1993). The second sample consisted of 78 embedded stars detected in the infrared by Wilking, Lada, & Young (1989) (18 of which are in common with the first sample). They found the MSDC of the H $\alpha$  sample had a power-law slope of  $-2.5 \pm 0.3$  on small scales ( $\lesssim 5000$  AU) and a slope of  $-0.36 \pm 0.06$  on large scales. The embedded sample had a slope of  $-0.28$  on large scales and combining the samples gave a slope of  $-0.26$  on large scales.

The slopes on small scales are consistent with binaries having an approximately uniform distribution of separations with the logarithm of separation. However, as described in Sections 3.2 and 4.1, when studying the large-scale distribution of stars in a SFR, it is essential to have the positions of the majority of the young stars in the survey region. Unfortunately, as demonstrated by the three different samples used by Simon (1997) and Nakajima et al. (1998), there is no complete sample of young pre-main-sequence stars available for Ophiuchus at this time (unlike for Taurus-Auriga). Another survey is that of Strom, Kepner, & Strom (1995) who find 119 pre-main-sequence stars, in three rich aggregates of young stars in the Ophiuchus cloud along with a more distributed population. Therefore, we prefer to wait until a more comprehensive list of young pre-main-sequence stars is available.

There are several comments to be made about the current analyses, however. First, the power-law slopes on large scales found by Nakajima et al. (1998) are quite flat and may be even flatter since they do not take into account boundary effects when calculating the MSDC (see Section 4.3). Second, for the embedded stars the power-law slope is calculated over separations from  $\approx 3000 - 65000$  AU. A flat MSDC on these scales is not unexpected since with a velocity dispersion of  $1 \text{ km s}^{-1}$ , any initial structure would be erased on these scales in  $\approx 3 \times 10^5$  years. Finally, the effects of the evolution of the MSDC with age may be apparent in the different samples used by Nakajima et al. (1998). The H $\alpha$  sample is presumably older than the embedded sample, is more dispersed, and has a lower mean surface density. This clearly results in a nearest-neighbour distribution which is

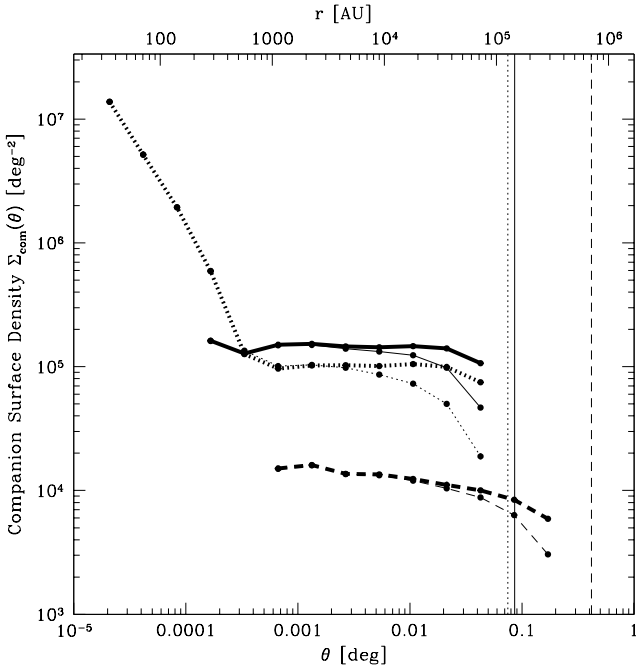


**Figure 15.** The mean surface density of companions  $\Sigma_{\text{com}}(\theta)$  for the stellar distributions from the surveys of the Orion Trapezium Cluster by Jones & Walker (1988) (dashed lines), Prosser et al. (1994) (dotted lines) and McCaughrean et al. (1996) (solid lines). In each case, the MSDC is calculated using Method 1 (thin lines), ignoring the effects of boundaries, and using Method 5 (thick lines) which attempts to correct for the boundaries of the survey regions. The vertical lines give the smallest dimension of the survey regions.

non-Poisson when the two samples are combined, regardless of whether or not there is sub-structure in the stellar distributions. To determine whether or not there is structure (e.g. sub-clustering or self-similar structure) in the distribution of forming stars, it is important to consider the youngest stars and the largest possible area. The youngest stars should be selected to minimise the erasure of structure (Section 3.3.1) and to avoid washing out any structure with a more uniform, older population (e.g. Figure 8). A large area allows the large-scale MSDC to be studied over the greatest possible range of separations. Note also that infrared surveys are preferred over optical, since they give greater completeness and minimise the problem of finding structure that is due to obscuration of stars by molecular gas rather than structure in the distribution of the stellar objects themselves.

#### 4.3 Orion Trapezium Cluster

Finally, Simon (1997) studied the spatial distribution of the Orion Trapezium Cluster, using the sample of 319 stars listed by Prosser et al. (1994) from their optical wavelength Hubble Space Telescope study which probed for binaries down to  $\approx 0.05''$  or  $\approx 25$  AU separation. As with the Taurus-Auriga and Ophiuchus SFRs, Simon (1997) found the MSDC on small-scales ( $\lesssim 1''$ ) is consistent with binaries having an approximately uniform distribution of separations with the logarithm of separation (with a power-law slope of  $-2.1 \pm 0.6$ ). On large-scales (2.5 to  $40''$ ), Simon found the

**Figure 16.** The stellar distributions from the surveys of the Orion Trapezium cluster by Jones & Walker (1988), Prosser et al. (1994) and McCaughrean et al. (1996).

MSDC could be described by a power-law slope of  $-0.2 \pm 0.2$ . Nakajima et al. (1998) studied the whole Orion A region and found a similar slope ( $-0.23 \pm 0.02$ ) to Simon. However, the Orion A region has a much larger spatial extent than the Orion Trapezium Cluster itself and therefore is not directly comparable to Simon's results or those presented here.

Figure 15 gives the MSDC for the data of Prosser et al. over the full range of separations, calculated using Method 1 (thin, dotted line) and Method 5 (thick, dotted line). The MSDC for separations  $\gtrsim 10''$  is entirely dependent on the corrections applied because of the boundaries of survey area. Fitting a power-law slope to the MSDC given by Method 1 over the same large-scale range as Simon ( $\approx 3 - 50''$ ) gives a slope of  $-0.17 \pm 0.03$  in agreement with Simon (we obtain a smaller standard error since we do not attempt to give error estimates for each MSDC value). However, using Method 5, the slope is  $0.01 \pm 0.01$  over both the range used by Simon and over the larger range of  $1.6 - 100''$ . Thus, Simon's conclusion that the power-law slope in the large-scale regime is the same in the Trapezium Cluster as in Taurus-Auriga appears to be based entirely on boundary effects (although we note that a slope of zero is within  $1\sigma$  of Simon's result due to his large error estimate). In a similar manner, since Nakajima et al. (1998) use the same method as Simon to calculate the MSDC, their large-scale power-law slopes are also likely to overestimate in magnitude.

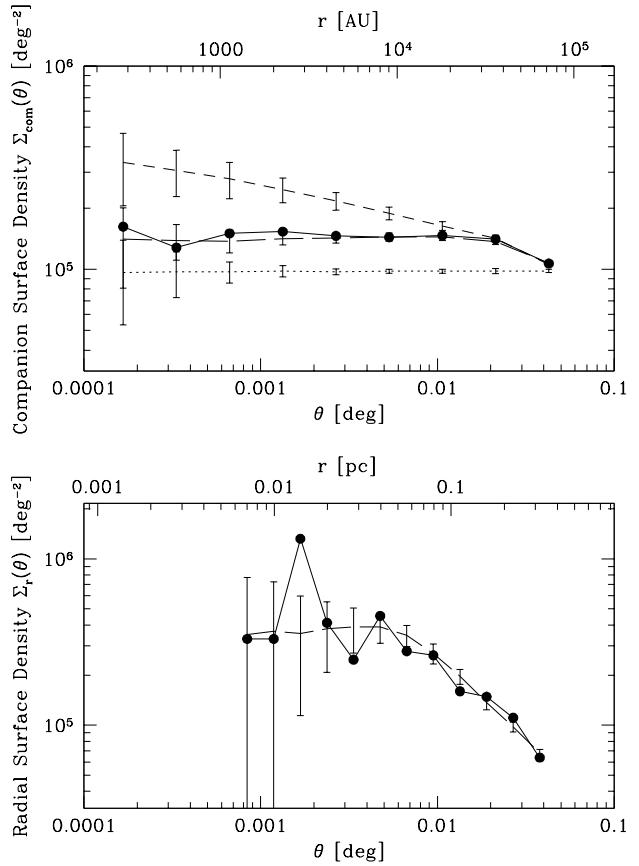
To better analyse the Trapezium Cluster, at least on the larger scales, we must turn to other data sets for several reasons. First, the Prosser et al. (1994) data cover a relatively limited part of the central cluster, albeit omitting the highest-density region including the Trapezium stars themselves. Second, the survey was at optical wavelengths, making it possible that younger, more embedded cluster members were missed. Finally, the survey boundary is very irregular making it difficult to correct the MSDC for boundary effects and raising the possibility that, if structure is found on large scales, it may simply be due to the non-uniform sampling of the cluster.

Figure 16 shows the coverage of the Prosser et al. survey and two alternate surveys. The first is that of McCaughrean et al. (1996) who imaged the central  $5' \times 5'$  of the cluster at  $2\mu\text{m}$ . The completeness limit was  $K = 17^m$ , and the steep turnover in the luminosity function at  $K \sim 12^m$  ensures that the sample of 744 sources is very complete, at least to systems more widely separated than the  $0.7''$  resolution limit. The second sample is that of Jones & Walker (1988) who carried out a ground-based optical photographic survey out to roughly  $15'$  from the centre of the Trapezium, (i.e. a much larger area than the other two samples). The sample contains 858 stars with  $\geq 90\%$  probability of being proper-motion members of the Orion complex. However, overall it is a less complete sample, with shallower detection and coarser resolution limits respectively.

The MSDC of all three surveys are given in Figure 15. The agreement between the large-scale MSDCs produced with the data of Prosser et al. (1994) and McCaughrean et al. (1996) is good because the two surveys contain a lot of overlap. The McCaughrean MSDC is higher overall primarily due to the inclusion of the high-stellar-density region centred on the Trapezium, while the Prosser MSDC reaches to smaller separations due to the superior resolution. Finally, notice that the boundary correction has less effect on the McCaughrean MSDC than on the Prosser MSDC because the former has more uniform coverage than the latter. Fitting a power-law slope to the McCaughrean MSDC over the range  $1.6 - 100''$  gives a slope of  $-0.11 \pm 0.02$  (Method 1) or  $-0.02 \pm 0.01$  correcting for boundary effects (Method 5). The MSDC of the Jones & Walker (1988) data is lower overall primarily due to the lack of completeness (and thus the lower stellar surface density), but also because the data extends out much farther where the stellar density (even correcting for completeness) is much lower and this lowers the *mean* surface density of companions. Unlike the Prosser and McCaughrean MSDCs (which are essentially flat outside the binary regime using Method 5), the Jones & Walker MSDC is fit by a small power-law slope of  $-0.17 \pm 0.03$  (Method 1) or  $-0.16 \pm 0.01$  (Method 5) over the range  $1.6 - 400''$ .

In previous sections we have seen that a sloping MSDC can result from many different effects (e.g. boundaries, global density profiles, clusters, and fractal stellar distributions). Thus, rather than interpreting the Trapezium Cluster large-scale MSDCs simply by fitting power-laws, we choose to compare the MSDCs with those of model stellar distributions. We assume a distance of 480 pc to the Trapezium Cluster (Genzel et al. 1981). Due to the superior datasets in the large-scale regimes, we only consider the data of McCaughrean et al. (1996) and of Jones & Walker (1988). Also, from this point on, we use Method 5 to calculate the MSDC, although since we are modelling the MSDC, rather than deriving slopes, this choice is unimportant.

Figure 17a gives the MSDC of the McCaughrean et al. data, along with the MSDC for three model stellar distributions. In the first model distribution (dotted line), 744 stars are distributed uniformly over the survey region. This results in an MSDC that is too low to fit the Trapezium Cluster data. In the second, 744 stars are distributed randomly with the volume density distribution of a singular isothermal sphere ( $\rho \propto r^{-2}$ ). Assuming the depth of the cluster is much greater than the radius of the survey region this is equivalent to the radial surface density distribution  $\Sigma_r(r) \propto r^{-1}$ .



**Figure 17.** The upper graph a), gives the mean surface density of companions  $\Sigma_{\text{com}}(\theta)$  for the McCaughrean et al. (1996) survey (points and solid line), along with the MSDC of three models: a uniform distribution of stars (dotted line); a singular isothermal sphere (short-dashed line); and a stellar distribution given by equation 13 (long-dashed line). The lower graph b), gives the radial surface density  $\Sigma_r(\theta)$  of the McCaughrean et al. survey along with that of the stellar distribution given by equation 13.

This time the MSDC is too high (short-dashed line), and has a slope that is inconsistent with the Trapezium Cluster data.

In Figure 17b, the radial surface density profile  $\Sigma_r(r)$  is given for McCaughrean et al. data. A good fit is obtained (long-dashed line) if the stars of the Trapezium Cluster are assumed to be distributed with a core of uniform volume density and  $\rho \propto r^{-2}$  outside the core

$$\rho(r) = \begin{cases} \rho_0 & \text{if } r \leq R_{\text{core}}, \\ \rho_0 \left(\frac{R_{\text{core}}}{r}\right)^2 & \text{if } r > R_{\text{core}} \end{cases} \quad (13)$$

with  $R_{\text{core}} = 30''$  and assuming that the depth of the three-dimensional distribution is much greater than the radius of the survey region. With 744 stars distributed within the survey area of McCaughrean et al. this gives a stellar density of  $\rho_0 = 2.1 \times 10^4 \text{ pc}^{-3}$  in the central core which is in good agreement with the value of  $1.7 \times 10^4 \text{ pc}^{-3}$  derived by Hillenbrand & Hartmann (1998) who fit a King model to the cluster, but less than the estimate of  $5 \times 10^4 \text{ pc}^{-3}$  by McCaughrean & Stauffer (1994) who fit the cluster with a King model with a smaller core radius. The MSDC of this stellar distribution is in excellent agreement with that of the

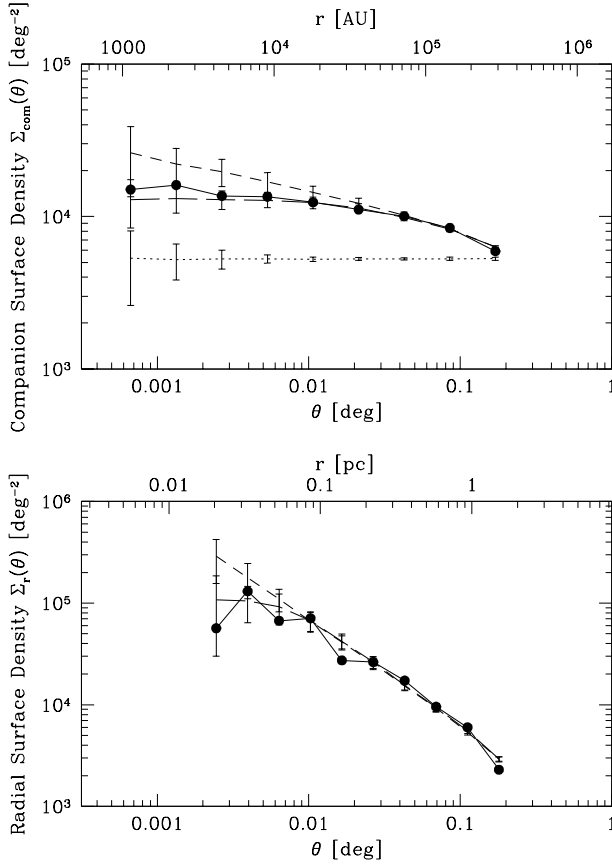


**Figure 18.** The upper graph a), gives the mean surface density of companions  $\Sigma_{\text{com}}(\theta)$  for the Jones & Walker (1988) survey (points and solid line), along with the MSDC of three models: a uniform distribution of stars (dotted line); a singular isothermal sphere (short-dashed line); and a stellar distribution given by equation 13 (long-dashed line). The lower graph b), gives the radial surface density  $\Sigma_r(\theta)$  of the Jones & Walker survey along with those of the singular isothermal sphere and the stellar distribution given by equation 13.

Trapezium Cluster data (Figure 17a). Thus, the distribution of stars in the central  $5' \times 5'$  of the Trapezium Cluster can be well described by this approximate non-singular isothermal sphere. In particular, *there is no evidence of sub-clustering or fractal structure*. Note also, that stellar densities given by this model and the lack of structure in the stellar distribution make the cluster three-dimensional in the sense of Section 3.1 (i.e.  $Z \gg d_3$ ). Thus, the break between the binary and the large-scale regimes in the Prosser MSDC cannot be associated with the typical Jeans length, even if the stellar distribution had not evolved since the stars formed (see Section 4.3.1).

In Figure 18a, the MSDC of Jones & Walker's Trapezium Cluster data is compared to the same three stellar distributions as the McCaughrean et al. data, except this time 858 stars are distributed over the survey area of Jones & Walker. Also, the approximation that the depth of the cluster is much greater than the radius of the survey region is no longer a good one. Therefore, we assume that the Jones & Walker survey covered most of the Trapezium Cluster and take the three-dimensional radius of the cluster to be

**Figure 19.** The mean surface density of companions  $\Sigma_{\text{com}}(\theta)$  for models of the Orion Trapezium Cluster with stars distributed in sub-clusters. The models are compared to the MSDC of the McCaughrean et al. (1996) survey (points). In each model, the stars or sub-cluster centres are distributed according to equation 13 and the sub-clusters each contain 10 stars which are distributed uniformly within a sphere of radius  $R_{\text{clus}}$ . The models have: 100% of stars in sub-clusters with  $R_{\text{clus}} = 3000$  AU (top left, dotted line); 10% of stars in sub-clusters with  $R_{\text{clus}} = 3000$  AU (top right, solid line); 100% of stars in sub-clusters with  $R_{\text{clus}} = 10^4$  AU (lower left, dashed line); 100% of stars in sub-clusters with  $R_{\text{clus}} = 3 \times 10^4$  AU (lower right, long-dashed line).

only twice the Jones & Walker survey radius of  $15'$ . As for the McCaughrean MSDC, the uniform-density stellar distribution is inconsistent with the Jones & Walker MSDC. It is more difficult to distinguish between the pure singular isothermal sphere and the distribution given by equation 13 with the Jones & Walker MSDC than it was with the McCaughrean MSDC, but equation 13 does provide a better fit. Figure 18b gives the radial surface density profile. Both the singular isothermal sphere and equation 13 provide reasonable fits to the radial surface density profile, although again equation 13 is preferred. In conclusion, the MSDCs of the surveys of McCaughrean et al. and Jones & Walker give *no*

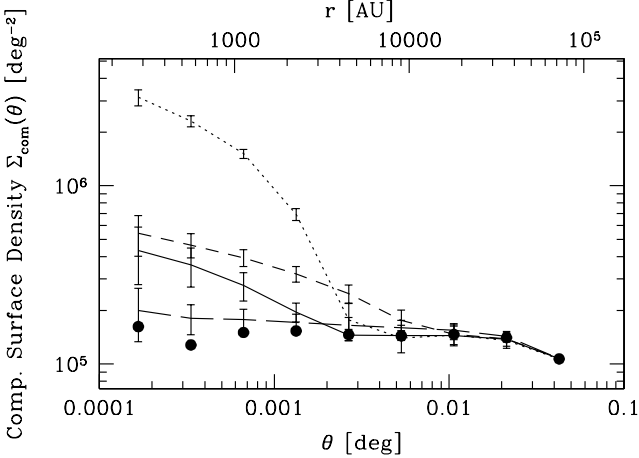


**Figure 20.** The same as in Figure 19 but with centrally-condensed sub-clusters with stars distributed inside the radius  $R_{\text{clus}}$  according to  $\rho \propto r^{-2}$ .

evidence for sub-clustering or fractal structure in the Orion Trapezium Cluster.

#### 4.3.1 Sub-clustering

Although we have shown that there is no evidence from the MSDC for hierarchical structure or sub-clustering of the stars in the Orion Trapezium Cluster, it is of interest to determine what *limits* can be placed on the presence of such structure. By generating model stellar distributions which contain stellar sub-clusters and comparing their MSDCs to that of the McCaughrean et al. (1996) survey, we can set limits on how much sub-clustering can be present.

Figure 19 compares the MSDCs of four different stellar distributions containing stars in sub-clusters to the MSDC of the McCaughrean et al. survey. In each case single stars, and/or the centres of sub-clusters, are distributed randomly according to equation 13. A total of 744 stars are allocated, some fraction of which are in sub-clusters. Each sub-cluster consists of 10 stars randomly distributed within the sub-cluster's radius  $R_{\text{clus}}$ . Comparing the models to the McCaughrean MSDC shows that the ease with which sub-clusters are detected depends on the total fraction of the stars that are in such sub-clusters and the radii of the sub-clusters. For example, the MSDC produced when 100% of the stars are in sub-clusters of radii 3000 AU is clearly inconsistent with the Trapezium Cluster data (dotted line). Detecting if 10% of the stars are in such sub-clusters, however, is more difficult (solid line). For sub-clusters with radii of  $10^4$  AU, any less than 100% of the stars being in such sub-clusters becomes difficult to detect (short-dashed line). Finally, it is impossible to detect whether or not *all* the stars are in sub-clusters with radii of  $3 \times 10^4$  AU (long-dashed line). Looking at the examples of each type of clustering in Figure 19, we note that the MSDC appears to be slightly less sensitive than the human eye for detecting sub-clustering, since the eye finds it easy to detect clustering in the  $R_{\text{clus}} = 10^4$  AU case while the MSDC detection is only  $2-3\sigma$  (see also Figure 6). The advantage of the MSDC over

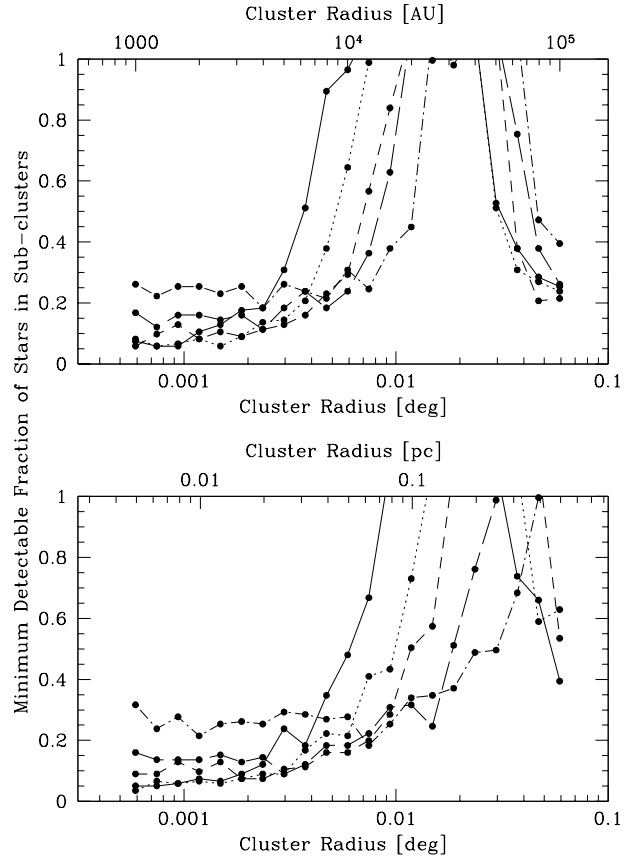


**Figure 21.** The minimum fraction of stars in sub-clusters that are detectable by comparing the MSDC of model stellar distributions to that of the McCaughrean et al. (1996) data. The minimum fraction that can be detected depends on the radii and number of stars within the sub-clusters and the degree of central condensation of the sub-clusters. In the upper graph a), the sub-clusters have a uniform stellar density while in the lower graph b), the sub-clusters have a  $\rho \propto r^{-2}$  stellar distribution. The sub-clusters contain 5 (solid lines), 10 (dotted lines), 20 (dashed lines), 40 (long-dashed lines) or 80 (dot-dashed lines) stars.

the eye, however, is that it is unbiased (the eye is good at seeing patterns where none exist) and gives a reproducible measure of the sub-structure.

The detection of sub-clustering also depends on the central condensation of the sub-clusters themselves. In Figure 20, the models are identical to those in Figure 19, except that the sub-clusters are centrally condensed with the 10 stars distributed randomly according to  $\rho \propto r^{-2}$ . Centrally-condensed sub-clusters are easier to detect than uniform-density sub-clusters.

In Figure 21, we give the minimum fraction of stars that are required to be in sub-clusters for the resulting MSDC to be inconsistent with the McCaughrean MSDC. The minimum fraction is a function of the degree of central-condensation of the sub-clusters, the number of stars in each sub-cluster (ranging from 5 to 80 stars per sub-cluster), and the radii of the sub-clusters (ranging from  $10^3$  to  $10^5$  AU). For example, in Figure 21a, a model with 100% of the stars being in sub-clusters of 5 stars (solid line) with  $R_{\text{clus}} = 2 \times 10^4$  AU gives an MSDC that is indistinguishable

from the McCaughrean MSDC, whereas if the sub-cluster radii are only  $R_{\text{clus}} = 1000$  AU, then a model with as few as 10% of the stars being in such clusters can be recognised as being different from the McCaughrean MSDC. A model MSDC is determined to be inconsistent with the McCaughrean MSDC if two or more bins differ from the McCaughrean MSDC values by more than  $2\sigma$ . The easier detection of more centrally-condensed sub-clusters is apparent (c.f. Figures 21a and 21b). For uniform-density sub-clusters, strong limits ( $\lesssim 30\%$ ) can be placed on the maximum fraction of stars in sub-clusters with  $R_{\text{clus}} \lesssim 6000$  AU. For centrally-condensed sub-clusters, strong limits ( $\lesssim 30\%$ ) can be placed on the maximum fraction of stars in sub-clusters with  $R_{\text{clus}} \lesssim 10000$  AU. The detection also depends on the number of stars in each sub-cluster. Finally, the possibility that a large fraction of the stars are in near-uniform-density sub-clusters with large radii ( $\gtrsim 5 \times 10^4$  AU) can be ruled out because the model stellar distributions are not as centrally-condensed as the Trapezium Cluster.

Although we cannot rule out all possible sub-clustering in the Trapezium Cluster, we emphasise that the McCaughrean MSDC is consistent with there being *no* sub-clustering. In fact, this is not too surprising. The stars in the Trapezium Cluster have a three-dimensional velocity dispersion of  $\approx 4$  km s $^{-1}$  (Jones & Walker 1988; Tian et al. 1996). If the stars formed in unbound associations, or in some type of hierarchical structure, in  $10^5$  years this velocity dispersion results in the stars typically drifting apart by  $\sim 10^5$  AU. Hence, any such primordial structure would have been destroyed by the current age of the Trapezium Cluster ( $\sim 10^6$  years) (Hillenbrand 1997). Note that this is not the case with the clustering that is observed in the Taurus-Auriga SFR. The smaller velocity dispersion of  $1-2$  km s $^{-1}$  (Hartmann et al. 1991) and large scale of the clustering ( $\approx 1$  pc) means that such structure takes  $\sim 10^6$  years to be destroyed.

On the other hand, if the Trapezium Cluster stars formed in bound sub-clusters, of  $10-100$  stars, there should still be some evidence. The maximum lifetime of such a sub-cluster is determined by its evaporation rate. For sub-clusters of  $10-100$  stars, the lifetime is  $\sim 100t_{\text{cross}}$  (Binney & Tremaine 1987), where  $t_{\text{cross}}$  is the crossing time. This gives the lifetime  $t$  of a sub-cluster of total stellar mass  $M_{\text{clus}}$  and radius  $R_{\text{clus}}$  to be

$$t \sim 3 \times 10^5 \left( \frac{M_{\text{clus}}}{10M_{\odot}} \right)^{1/2} \left( \frac{R_{\text{clus}}}{1000 \text{ AU}} \right)^{3/2} \text{ yr.} \quad (14)$$

Therefore, if the stars of the Trapezium Cluster formed in bound sub-clusters of  $10-100$  stars within  $R_{\text{clus}} \approx 10^3$  AU, they would have evaporated by the present time. However, sub-clusters with  $R_{\text{clus}} \gtrsim 10^4$  should have survived and would be relaxed (centrally-condensed). From Figure 21, it is possible that such bound sub-clusters exist in the Trapezium Cluster, but they cannot be detected by modelling the MSDC.

#### 4.3.2 Binaries

Thus far, we have concentrated on large-scale structure in the Orion Trapezium Cluster. While the survey of Jones & Walker (1988) does not extend to small enough separations to detect binaries above the confusion limit in the Trapezium

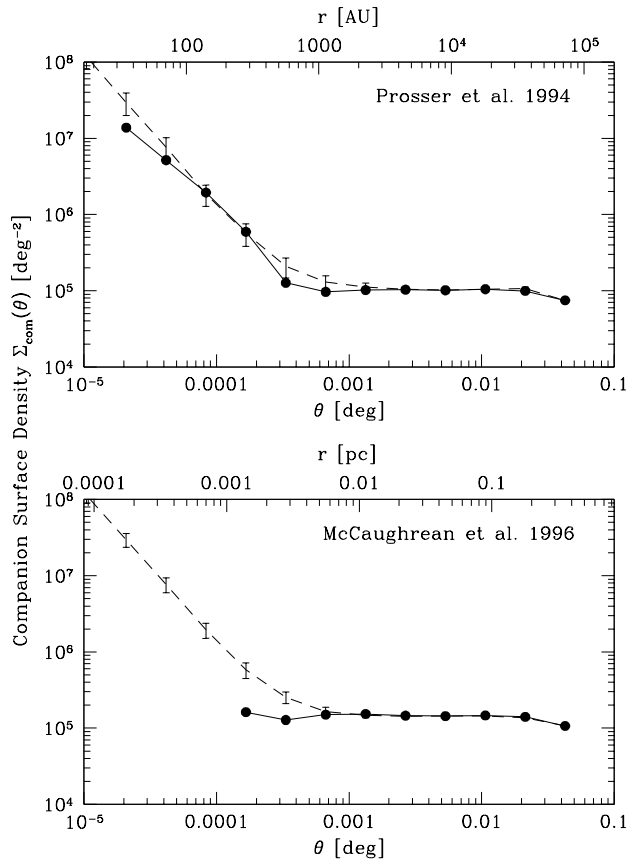


**Figure 22.** The mean surface density of companions  $\Sigma_{\text{com}}(\theta)$  for the Orion Trapezium Cluster using the data of Prosser et al. (1994) (top, points and solid-line) and McCaughrean et al. (1996) (bottom, points and solid-line). The observations are fit by  $\Sigma_{\text{com}}(\theta)$  of the three-dimensional stellar system distribution given by equation 13, with 36% of the systems being binaries with separations in the range 10 to  $10^4$  AU (see text).

Cluster, the surveys of McCaughrean et al. (1996) and, especially, of Prosser et al. (1994) do. In Figure 22 we model the Trapezium Cluster MSDC, taking into account binaries. We distribute stellar systems according to equation 13, where each stellar system is randomly chosen to be either a single star or a binary with a separation in the range 10 to  $10^4$  AU. Such large maximum binary separations are possible even though the break between the binary and large-scale regimes occurs at  $\approx 600$  AU since, as seen in Section 3.1, the break does not necessarily give the maximum binary separation and in the Trapezium Cluster, as seen above, the break is not associated with the Jeans length. The ratio of binary systems to the total number of systems is 0.36, which corresponds to a binary frequency of 60% if binaries have separations between 0.1 and  $10^4$  AU that are distributed as in equation 2. For each survey (the Prosser et al. survey and the McCaughrean et al. survey) the stars are distributed over the same areas as the surveys, and we ensure that the total number of stars (not systems) is the same as in each survey.

The fact that the stellar distribution used to model the McCaughrean MSDC contains systems that would not have been resolved in the survey of McCaughrean et al. does not

matter. What is important is that the same number of stars are used for the calculation of both MSDCs (to give the correct normalisation) and that the stars that are in close binaries are placed according to the same large-scale spatial distribution as the other stars (which, of course, they are). An alternative method is to allocate the same number of resolvable systems in the model distribution as is observed, and then to multiply the model MSDC by the number of observed stars and divide by the number of stars in the model to get the correct normalisation.

The model gives an excellent fit to *both* sets of Trapezium Cluster data (Figure 22) which is particularly pleasing since equation 13 was derived from fitting only the McCaughrean MSDC and radial density profiles (not the Prosser et al. data). The overall binary frequency of 60% was chosen because this agrees with that of the field stars (Duquennoy & Mayor 1991) which in turn is consistent with the binary frequency that Prosser et al. derived for their data.

The only regions that are not so well fit are the region between about 0.8 and 2'' (400 to 1000 AU) and the two smallest separation bins of the Prosser MSDC where the Trapezium Cluster has a lower MSDC than predicted. The latter of these regions can be explained by incompleteness for binaries with close separations. The deficit between 400 and 1000 AU, however, gives *very weak* evidence that binaries with separations  $\gtrsim 500$  AU may have been depleted by binary-single interactions in the centre of the Trapezium Cluster (e.g. Kroupa 1995a,b,c). A simple calculation of the timescale for such encounters (Binney & Tremaine 1987) shows that this is possible. Assuming a central stellar density of  $2 \times 10^4 \text{ pc}^{-3}$  (Section 4.3; Hillenbrand & Hartmann 1997) and a three-dimensional stellar velocity dispersion of  $4 \text{ km s}^{-1}$  (Jones & Walker 1988; Tian et al. 1996), the timescale for a star to have an encounter at 500 AU is  $\approx 7 \times 10^5$  years which is of the same order as the age of the Trapezium Cluster (Hillenbrand 1997).

## 5 CONCLUSIONS

We have studied the interpretation of the mean surface density of companions (MSDC) as a function of separation  $\Sigma_{\text{com}}(\theta)$  in star-forming regions. We have shown how the power-law slope of  $\approx -2$  for binaries is due to their flat distribution of periods in the logarithm of separation, and have considered the MSDC of various global density profiles, sub-clusters and self-similar distributions. We emphasise that simply because a power-law slope can be fit to a particular MSDC, it does not mean that the stellar distribution is self-similar or fractal. We have also demonstrated the effects of survey boundaries on the calculation of  $\Sigma_{\text{com}}(\theta)$ . Several methods of attempting to avoid boundary effects were considered, all of which provide a full correction in the case that there is no large-scale stellar density gradient across boundaries, but none of which give a perfect correction when there are such large-scale gradients. Of these, we recommend Method 5, since it allows the maximum range of separations to be studied, does not discard any information, and is simple to use for surveys with irregular boundaries. Even in the case of a uniform stellar distribution, the improper handling of boundaries results in the  $\Sigma_{\text{com}}(\theta)$  having

a significant slope for separations greater than  $\approx 1/50$  of the survey area's dimensions (i.e. using Method 1).

Larson (1995) associated the separation at which a break in  $\Sigma_{\text{com}}(\theta)$  between the binary regime and the large-scale regime occurs with the Jeans length in the Taurus-Auriga star-forming region (SFR). However, we show this transition separation may only be associated with the Jeans length in special cases, and that the transition separation does not necessarily give the maximum binary separation. In general, the break occurs at the separation where the mean surface density of *binary* companions is equal to the mean surface density of *non-binary* companions (the latter of which may be physically close, or simply chance projections). Thus, typically, the break occurs at smaller separations for SFRs with higher stellar surface densities (as observed by Simon (1997) and Nakajima et al. (1998)). In turn, the surface density of non-binary companions depends on the parameters of the binaries, the volume density of stars, the volume-filling factor of the stellar distribution and, in general, the depth of the star-forming region.

The transition separation between the binary and the large-scale regimes also evolves with time. Due to a stellar velocity dispersion, initial structure is erased and the surface density of stars in an unbound region generally decreases. This effect begins at the smallest scales, extends to larger scales with time, and results in the transition separation increasing with time. Finally, the transition between the binary and the large-scale regimes may allow a truncation of binaries at large separations to be detected, especially in old clusters that were much denser when the stars were formed and have since expanded. In such cases, this provides a record of the stellar density when the stars first formed.

In summary, the transition separation may be associated with the Jeans length only if the star-forming region is young enough that initial structure has not been erased, and if the SFR is 'optically thin' in the sense that projection effects due to the depth of the SFR do not affect the transition separation. The latter is true if the volume-filling factor of the SFR is low (e.g. the SFR is composed of widely separated clusters consisting of only a few stars ( $\sim 10$ ), or if the stars have a fractal distribution with dimension  $\lesssim 1.5$ ). This is the case for the Taurus-Auriga SFR, which explains the good agreement between the transition separation and the Jeans length found by Larson (1995), but it is not the case for the Orion Trapezium Cluster.

It is important when studying the large-scale spatial distributions of star-forming regions to obtain the most complete sample of stars over the largest area possible. The lack of such data for the Ophiuchus SFR makes an attempt to study its large-scale spatial distribution of little use at this time.

For the Taurus-Auriga and Orion Trapezium SFRs, the current data makes a meaningful study of their large-scale stellar distribution possible. For the Taurus-Auriga SFR, Larson (1995) fit the large-scale MSDC with a power-law slope that implied a fractal stellar distribution. However, this is not the only possible interpretation; the data can be equally well fit by assuming the stars are formed primarily in randomly-distributed clusters of stars. For the Orion Trapezium SFR, we find that the MSDC is consistent with the stars simply being distributed according to a surface density that decreases with radius; there is no evidence for

sub-structure (either fractal or sub-clusters) in the stellar distribution. We also demonstrate how upper limits can be placed on how much sub-clustering is present, and note the sensitivity of the MSDC to detecting sub-structure appears to be slightly less than that of the human eye. The results for the Orion Trapezium SFR are consistent with the fact that if structure were present when the stars formed, it would have been erased by the current time due to the stellar velocity dispersion.

Binaries in the Taurus-Auriga and Orion Trapezium SFR are roughly consistent with an MSDC with a power-law slope of  $\approx -2$ . However, we point out that comparing power-law indices derived from the slope of the MSDC in the binary regime is not the best way to compare the distribution of binary separations between stellar populations since any structure or deviation from a true power-law may easily be missed. In the centre of the Orion Trapezium SFR, we find very weak evidence that there may be a deficit of binaries with separations  $\gtrsim 500$  AU. Such a deficit may be caused by the disruption of wide binaries by single-binary star encounters.

Finally, in view of our studies of the Taurus-Auriga and Orion Trapezium SFRs, we emphasise caution when interpreting the MSDC. Rather than attempting to characterise star-forming regions simply by fitting power-laws to  $\Sigma_{\text{com}}(\theta)$ , it is more instructive to also consider the global stellar distribution (e.g. a radial surface density profile) and to compare the MSDC to those of model stellar distributions to determine the robustness of any conclusions. Alternatively, rather than just considering the MSDC (or, equivalently, the two-point correlation function), correlation functions of higher order (three and four-point correlation functions) and/or the nearest-neighbour distribution can be used to differentiate between non-hierarchical and hierarchical structure. The use of higher-order correlation functions is common in studying the large-scale structure of the universe (Peebles 1980). The nearest-neighbour distribution has been used by Nakajima et al. (1998) to argue that the power-law slope of an MSDC on large scales may indicate a stellar age spread rather than the presence of hierarchical structure. However, while an age spread does help explain their results, we argue that their results do not exclude the possibility that stars form in hierarchical structures. More work is required on this topic.

## ACKNOWLEDGMENTS

We are grateful to Richard Larson, Mike Simon, and the referee, Lee Hartmann, for their critical reading of the manuscript and comments which helped improve this paper. We also thank Michael Meyer, Ralf Klessen, Ian Bonnell, and Melvyn Davies for useful discussions.

## REFERENCES

Binney J., Tremaine S., 1987, *Galactic Dynamics*. Princeton University Press, Princeton, p. 489-491

Duquennoy A., Mayor M., 1991, *A&A*, 248, 485

Fischer D. A., Marcy G. W., 1992, *ApJ*, 396, 178

Genzel R., Reid M. J., Moran J. M., Downes D., 1981, *ApJ*, 244, 884

Ghez A. M., Neugebauer G., Matthews K., 1993, *AJ*, 106, 2005

Gomez M., Hartmann L., Kenyon S., Hewitt R., 1993, *AJ*, 105, 1927

Hartmann L., Jones B. F., Stauffer J. R., Kenyon S. J., 1991, *AJ*, 101, 1050

Hillenbrand L. A., 1997, *AJ*, 113, 1733

Hillenbrand L. A., Hartmann L. W., 1998, *ApJ*, 492, 540

Jones B. F., Walker M. F., 1988, *AJ*, 95, 1755

Kroupa P., 1995a, *MNRAS*, 277, 1491

Kroupa P., 1995b, *MNRAS*, 277, 1507

Kroupa P., 1995c, *MNRAS*, 277, 1522

Lada E. A., Strom K. M., Myers P. C., 1993, in Levy E. H., Lunine J. I., eds., *Protostars and Planets III*. Univ. Arizona Press, Tucson, p. 245

Larson R. B., 1995, *MNRAS*, 272, 213

Leinert Ch., Zinnecker H., Weitzen N., Christou J., Ridgeway S. T., Jameson R., Haas M., Lenzen R., 1993, *A&A*, 278, 129

Mayor M., Duquennoy A., Halbwachs J. -L., Mermilliod J. -C., 1992, in McAlister H. A., Hartkopf W. I., eds., *Complementary Approaches to Double and Multiple Star Research (IAU Colloquium 135)*. ASP, San Francisco, p. 73

McCaughrean M. J., Stauffer J. R., 1994, *AJ*, 108, 1382

McCaughrean M. J., Rayner J., Zinnecker H., Stauffer J., 1996, in Beckwith S., Staude J., Quetz A., Natta A., eds., *Disk and Outflows Around Young Stars (Lecture Notes in Physics 465)*. Springer, Heidelberg, p. 33

Nakajima Y., Tachihara K., Hanawa T., Nakano M., 1998, *ApJ*, 497, 721

Peebles P. J. E., 1980, *The Large-Scale Structure of the Universe*. Princeton University Press, Princeton, p. 138-256

Prosser C. F., Stauffer J. R., Hartmann L., Soderblom D. R., Jones B. F., Werner M. W., McCaughrean M. J., 1994, *ApJ*, 421, 517

Reipurth B., Zinnecker H., 1993, *A&A*, 278, 81

Simon M., 1992, in McAlister H. A., Hartkopf W. I., eds., *Complementary Approaches to Double and Multiple Star Research (IAU Colloquium 135)*. ASP, San Francisco, p. 41

Simon M., 1997, *ApJ*, 482, L81

Simon M., Ghez A. M., Leinert Ch., Cassar L., Chen W. P., Howell R. R., Jameson R. F., Matthews K., Neugebauer G., Richichi A., 1995, *ApJ*, 443, 625

Strom K. M., Kepner J., Strom S. E., 1995, *ApJ*, 438, 813

Tian K. P., Leeuwen F., Zhao J. L., Su C. G., 1996, *A&AS*, 118, 503

Wichmann R., Bastian U., Krautter J., Jankovics I., Ruciński S. M., 1998, *MNRAS*, submitted

Wilking B. A., Lada C. J., Young E. T., 1989, *ApJ*, 340, 823

Wilking B. A., Schwartz R. D., Blackwell J. H., 1987, *AJ*, 94, 106

Zinnecker H., McCaughrean M. J., Wilking B. A., 1993, in Levy E. H., Lunine J. I., eds., *Protostars and Planets III*. Univ. Arizona Press, Tucson, p. 429

This figure "fig01.gif" is available in "gif" format from:

<http://arxiv.org/ps/astro-ph/9804154v1>

This figure "fig03.gif" is available in "gif" format from:

<http://arxiv.org/ps/astro-ph/9804154v1>

This figure "fig04.gif" is available in "gif" format from:

<http://arxiv.org/ps/astro-ph/9804154v1>

This figure "fig06.gif" is available in "gif" format from:

<http://arxiv.org/ps/astro-ph/9804154v1>

This figure "fig08.gif" is available in "gif" format from:

<http://arxiv.org/ps/astro-ph/9804154v1>

This figure "fig09.gif" is available in "gif" format from:

<http://arxiv.org/ps/astro-ph/9804154v1>

This figure "fig10.gif" is available in "gif" format from:

<http://arxiv.org/ps/astro-ph/9804154v1>

This figure "fig13.gif" is available in "gif" format from:

<http://arxiv.org/ps/astro-ph/9804154v1>

This figure "fig16.gif" is available in "gif" format from:

<http://arxiv.org/ps/astro-ph/9804154v1>

This figure "fig19.gif" is available in "gif" format from:

<http://arxiv.org/ps/astro-ph/9804154v1>